Flow computation based on kinematics

3

Flows can be classified according to the vorticity distribution as *irrotational flows* if the vorticity vanishes or is nearly zero throughout the domain of flow, *vortex flows* dominated by the presence of compact regions of concentrated vorticity embedded in an otherwise irrotational fluid, and *rotational flows* if the vorticity is significant throughout the domain of flow. In this chapter, we discuss the kinematic structure and mathematical description of the simplest and most tractable class of irrotational flows.

Following the mathematical analysis, we will develop finite-difference methods for computing the velocity field from knowledge of the velocity distribution at the boundaries, and then present a class of elementary irrotational flows that serve as fundamental building blocks for generating desired solutions. Complementary building blocks associated with elementary vortex flows provide us with additional elementary units that allow us to address a broader class of irrotational flows where the fluid exhibits circulatory motion.

3.1   Flow classification based on kinematics

In Chapters 1 and 2, we discussed the general kinematic properties of a flow with reference to the motion of fluid parcels and infinitesimal point particles. To make further progress, we establish a taxonomy by classifying flows according to sensible criteria. Examples of possible classifications include internal and external flows, inviscid and viscous flows, subsonic and supersonic flows.

On the basis of kinematics alone, flows can be classified into three main categories, including irrotational flows, flows containing compact regions of intense vorticity embedded in an otherwise perfectly or nearly irrotational fluid, and rotational flows with distributed vorticity.

Irrotational flows

The first category includes flows where the vorticity vector vanishes, and the magnitude of the vorticity is zero throughout the domain of flow. According to our discussion in Chapter 2, small spherical fluid parcels in a three-dimensional irrotational flow and discoidal fluid parcels in a two-dimensional irrotational flow translate, deform, and expand or contract, but do not rotate.

A perfectly irrotational flow is a mathematical idealization. In practice, because a small amount of vorticity is always present, a nominally irrotational flow is nearly but not perfectly irrotational. An example is high-speed flow past a slender airfoil under conditions of no-stall, as will be discussed in Chapter 12 in the context of aerodynamics.

Vortex flows

The second category includes flows that contain well-defined compact regions where the magnitude of the vorticity is significant, embedded in an otherwise irrotational fluid. The vortical flow regions cannot be neglected without introducing serious discrepancies and compromising the physics of the flow under consideration. In practice, regions of intense vorticity appear in the form of narrow layers, thin filaments, wakes behind bluff bodies, tornadoes and swirls. A vortex flow familiar to the aircraft traveler is the flow associated with a high-speed jet emerging from a turbine engine.

Rotational flows

The third category includes flows where the vorticity is significant throughout the domain of flow. The distinction between vortex flows and rotational flows is somewhat vague, as some flows can be classified into both categories. However, we will see that vortex flows can be analyzed and computed using a special class of numerical methods, called vortex methods. The availability of these methods provides us with a practical criterion for the distinction between vortex and rotational flows.

Flows in nature and technology

The vast majority of flows in nature and technology are rotational. Examples include the flow due to a small particle settling in the atmosphere, the flow through the engine of a turbine, and blood flow in the heart and through large blood vessels and small capillaries. High-speed flows develop regions of concentrated vorticity and are typically classified as vortex flows. High-speed turbulent flows contain random collections of rapidly evolving vortices, called eddies or coherent structures, embedded in a low- or moderate-vorticity background fluid.

Irrotational flows are simplified models of vortex flows that emerge by neglecting the regions of concentrated vorticity, or else by shifting the actual boundaries of the flow to the edges of the vortex regions, thereby placing them outside the domain of flow.

Considerable physical insight and practical experience are necessary to accurately predict whether a flow will develop to become irrotational, rotational, or vortex flow. Insights can be gained by studying model flows that are amenable to analytical and simple numerical methods. Additional insights can be gained by analyzing the laws governing the generation and evolution of the vorticity field from a given initial state.

Flow computation

The difficulty of computing the structure or evolution of a flow increases sharply as we transition from irrotational flows, to vortex flows, to rotational flows. Exceptions to this general rule arise in special cases. Our discussion of analytical and computational methods for flow computation begins in this chapter by considering the most amenable class of irrotational flows. In the context of kinematics alone, the problem can be stated as follows: given the boundary geometry and the velocity distribution over the boundaries, compute the structure of a steady irrotational flow or the evolution of an unsteady irrotational flow from a specified initial state.

PROBLEM

3.1.1 *Flow classification*

Suggest a possible way of classifying flows according to sensible criteria apart from the those discussed in the text.

3.2   Irrotational flow and the velocity potential

The vorticity of a three-dimensional flow was defined in equation (2.3.8) as the curl of the velocity,

$$\boldsymbol{\omega} \equiv \boldsymbol{\nabla} \times \mathbf{u}. \tag{3.2.1}$$

The z component of the vorticity of a two-dimensional flow in the xy plane was given in equation (2.3.19) as

$$\omega_z = \frac{\partial u_y}{\partial x} - \frac{\partial u_x}{\partial y}, \tag{3.2.2}$$

and the azimuthal component of the vorticity of an axisymmetric flow was given in equation (2.3.22) as

$$\omega_\varphi = \frac{\partial u_\sigma}{\partial x} - \frac{\partial u_x}{\partial \sigma} = \frac{1}{r} \left(\frac{\partial(r u_\theta)}{\partial r} - \frac{\partial u_r}{\partial \theta} \right). \tag{3.2.3}$$

If a flow is irrotational, the structure of the velocity field must be such that the right-hand sides of these equations are zero.

3.2.1   Two-dimensional flow

Consider a two-dimensional irrotational flow in the xy plane. Setting the left-hand side of equation (3.2.2) to zero, we obtain a constraint on selected partial derivatives of the velocity,

$$\frac{\partial u_y}{\partial x} = \frac{\partial u_x}{\partial y}. \tag{3.2.4}$$

To describe a two-dimensional irrotational flow, we may attempt to compute the two velocity components individually, subject to constraints imposed by the continuity equation and boundary conditions, while ensuring that condition (3.2.4) is fulfilled at every point in the flow. Alternatively, we may choose to satisfy condition (3.2.4) at the outset and then concentrate on fulfilling the rest of the requirements.

It should not be surprising that the second approach is more expedient in both theoretical analysis and numerical computation.

The velocity potential

The key idea is to introduce a new scalar function, ϕ, called the velocity potential, such that the two velocity components of a two-dimensional flow derive from the relations

$$u_x = \frac{\partial \phi}{\partial x}, \qquad u_y = \frac{\partial \phi}{\partial y}. \tag{3.2.5}$$

In vector notation, equations (3.2.5) are collected into the compact form

$$\mathbf{u} = \boldsymbol{\nabla}\phi, \tag{3.2.6}$$

where

$$\boldsymbol{\nabla}\phi = \Big(\frac{\partial \phi}{\partial x}, \quad \frac{\partial \phi}{\partial y}\Big), \tag{3.2.7}$$

is the two-dimensional gradient of the potential. The velocity, and thus the velocity potential, ϕ, is a function of position, $\mathbf{x} = (x, y, z)$, and, in the case of unsteady flow, time, t. Inspection of (3.2.5) reveals that the velocity potential has units of velocity multiplied by length, which amounts to length squared divided by time.

It is a straightforward exercise to confirm that, if the velocity components derive from ϕ in terms of equations (3.2.5), then the irrotationality constraint (3.2.4) is automatically satisfied. Substituting expressions (3.2.5) into (3.2.4), we obtain

$$\frac{\partial^2 \phi}{\partial x \, \partial y} = \frac{\partial^2 \phi}{\partial y \, \partial x}. \tag{3.2.8}$$

Since the order of partial differentiation with respect to the two independent spatial variables, x and y, can be interchanged, relation (3.2.4) is satisfied. Accordingly, an irrotational flow is also a potential flow, and *vice versa*.

The velocity potential of a certain irrotational flow is not unique. An arbitrary constant can be added to a particular potential to produce another perfectly acceptable potential. However, this ambiguity is neither essential nor alarming. In performing analytical or numerical computation, the arbitrary constant is determined by introducing a proper constraint.

Deriving the potential

Given the velocity field of an irrotational flow, we can derive the corresponding potential by integrating the system of differential equations (3.2.5), where the left-hand sides are treated as a known.

As an example, we consider two-dimensional unidirectional streaming (uniform) flow with velocity components

$$u_x = U_x, \qquad u_y = U_y, \tag{3.2.9}$$

where U_x and U_y are two constant velocities. Integrating the first equation in (3.2.5), we find that the potential must take the form

$$\phi = U_x x + f(y), \tag{3.2.10}$$

where $f(y)$ is an unknown function of y. Differentiating both sides of this equation with respect to y and using the second equation in (3.2.5), we find that $df/dy = U_y$, which can be integrated to give $f(y) = U_y y + c$, where c is an arbitrary constant. Combining these expressions, we find that the velocity potential corresponding to (3.2.9) is

$$\phi = U_x x + U_y y + c = \mathbf{U} \cdot \mathbf{x} + c. \tag{3.2.11}$$

In agreement with our previous observation, the velocity potential is defined uniquely up to an arbitrary constant, c.

Computation of the potential based on kinematics

The automatic satisfaction of the irrotationality constraint (3.2.4) by way of the velocity potential is helpful, but we still require one equation, or a system of equations, that will allow us to compute the potential. Normally, these equations would have to be derived by considering forces and torques exerted on the surfaces and over the volume of small fluid parcels, as will be discussed in subsequent chapters with reference to the more general class of rotational flows. Fortunately, this is not necessary in the case of irrotational flow. Given the boundary distribution of the velocity, an irrotational flow can be computed in the framework of kinematics alone pivoted on the continuity equation.

3.2.2 Incompressible fluids and the harmonic potential

Mass conservation requires that the velocity field of an incompressible fluid is solenoidal, which means that the velocity components must satisfy the constraint expressed by the continuity equation (2.9.2),

$$\boldsymbol{\nabla} \cdot \mathbf{u} = 0. \tag{3.2.12}$$

In the case of two-dimensional flow, we obtain

$$\frac{\partial u_x}{\partial x} + \frac{\partial u_y}{\partial y} = 0. \tag{3.2.13}$$

Substituting expressions (3.2.5) into (3.2.12), we obtain Laplace's equation in two dimensions,

$$\frac{\partial^2 \phi}{\partial x^2} + \frac{\partial^2 \phi}{\partial y^2} = 0. \tag{3.2.14}$$

It is convenient to define the two-dimensional Laplacian operator,

$$\nabla^2 \equiv \frac{\partial^2}{\partial x^2} + \frac{\partial^2}{\partial y^2}, \tag{3.2.15}$$

and recast (3.2.14) into the more compact form

$$\nabla^2 \phi = 0. \tag{3.2.16}$$

A function that satisfies Laplace's equation (3.2.16) is called harmonic.

It is instructive to derive Laplace's equation working in vector notation. Substituting (3.2.6) into (3.2.12), we find that

$$\boldsymbol{\nabla} \cdot \mathbf{u} = \boldsymbol{\nabla} \cdot (\boldsymbol{\nabla}\phi) \equiv \nabla^2 \phi = 0, \tag{3.2.17}$$

which identifies the Laplacian operator with the divergence of the gradient,

$$\nabla^2 = \boldsymbol{\nabla} \cdot \boldsymbol{\nabla}, \tag{3.2.18}$$

regarded as a differential operator.

Laplace's equation arises in a broad range of contexts under and beyond the auspices of fluid mechanics. For example, Laplace's equation governs the distribution of temperature at steady state in a conductive material, such as a fin or a cooling plate.

Quasi-steady state

Laplace's equation (3.2.16) conveys a statement of mass conservation for an incompressible fluid. Although time does not appear explicitly in this equation, the velocity field, and thus the velocity potential, may change in time, so that $\phi(\mathbf{x}, t)$. The absence of explicit time dependence classifies an the irrotational flow of an incompressible fluid as a quasi-steady flow. This terminology implies that the instantaneous structure of the flow depends on the instantaneous boundary geometry and boundary conditions, but is independent of the motion at previous times. Thus, if all boundaries are stationary at a particular time instant, the fluid will also be stationary at that instant, independent of the history of the fluid and boundary motion.

3.2.3 Three-dimensional flow

The foregoing analysis can be extended in a straightforward fashion to three-dimensional flow. The velocity components of a three-dimensional flow derive from the velocity potential by the equations

$$u_x = \frac{\partial \phi}{\partial x}, \qquad u_y = \frac{\partial \phi}{\partial y}, \qquad u_z = \frac{\partial \phi}{\partial z}. \qquad (3.2.19)$$

The velocity components, and thus the potential, ϕ, are functions of position $\mathbf{x} = (x, y, z)$ and time, t, in the case of unsteady flow.

If the fluid is incompressible, the velocity potential satisfies the counterpart of Laplace's equation (3.2.17) for three-dimensional flow,

$$\boldsymbol{\nabla} \cdot \mathbf{u} = \boldsymbol{\nabla} \cdot (\boldsymbol{\nabla}\phi) \equiv \nabla^2 \phi \equiv \frac{\partial^2 \phi}{\partial x^2} + \frac{\partial^2 \phi}{\partial y^2} + \frac{\partial^2 \phi}{\partial z^2} = 0, \qquad (3.2.20)$$

where

$$\boldsymbol{\nabla}^2 \equiv \frac{\partial^2}{\partial x^2} + \frac{\partial^2}{\partial y^2} + \frac{\partial^2}{\partial z^2} \qquad (3.2.21)$$

is the Laplacian operator in three dimensions.

3.2.4 Boundary conditions

Laplace's equation for the velocity potential, ϕ, in two or three dimensions is a second-order, elliptic partial differential equation. One consequence of this classification is that, in order to compute the solution, we must specify one scalar boundary condition for ϕ, one of its first partial derivatives, or a combination thereof, along each boundary.

Impermeable boundaries

Over an impermeable boundary, we require the no-penetration condition discussed in Section 2.10. If the boundary is stationary, $\mathbf{u} \cdot \mathbf{n} = 0$, where $\mathbf{n}$ is the unit vector normal to the boundary pointing either into or outward from the domain of flow. Using equations (3.2.5), we find that

$$n_x \frac{\partial \phi}{\partial x} + n_y \frac{\partial \phi}{\partial y} = 0. \qquad (3.2.22)$$

in the case of two-dimensional flow. This is truly a boundary condition for the normal component of the gradient of the potential, which is equal to the derivative with respect to distance normal to the boundary, called a *Neumann boundary condition.* Because the right-hand side of (3.2.22) is zero, this boundary condition is classified as homogeneous.

Permeable boundaries

Over a permeable boundary, we may specify the tangential component of the velocity and allow the normal component to arise as part of the solution. To implement this condition in

the case of two-dimensional flow, we introduce the unit vector tangential to the boundary, $\mathbf{t}$, defined in equations (2.6.3). The tangential component of the velocity in the direction of $\mathbf{t}$ is given by the inner product

$$u_t \equiv \mathbf{u} \cdot \mathbf{t} = t_x \frac{\partial \phi}{\partial x} + t_y \frac{\partial \phi}{\partial y} = \frac{\mathrm{d}x}{\mathrm{d}\ell} \frac{\partial \phi}{\partial x} + \frac{\mathrm{d}y}{\mathrm{d}\ell} \frac{\partial \phi}{\partial y} = \frac{\mathrm{d}\phi}{\mathrm{d}\ell}, \qquad (3.2.23)$$

where ℓ is the arc length measured in the direction of $\mathbf{t}$. If the distribution of ϕ over the boundary is known, the right-hand side of (3.2.23) can be computed by differentiating the potential with respect to arc length using analytical or numerical methods.

The last observation suggests that, instead of specifying the tangential component of the velocity, we may specify the boundary distribution of the potential. A boundary condition for the distribution of the potential is a *Dirichlet boundary condition.*

A word of caution is in order. If a flow is bounded by a number of disconnected boundaries, replacing the boundary condition for the tangential velocity with a boundary condition for the distribution of the potential is permissible only over one boundary; otherwise, inconsistencies may arise.

3.2.5   Cylindrical polar coordinates

Consider a three-dimensional irrotational flow and introduce cylindrical polar coordinates, (x, σ, φ), as shown in Figure 1.3.2. Using expressions (2.1.43), we find that the cylindrical polar components of the velocity are given by

$$u_x = \frac{\partial \phi}{\partial x}, \qquad u_\sigma = \frac{\partial \phi}{\partial \sigma}, \qquad u_\varphi = \frac{1}{\sigma} \frac{\partial \phi}{\partial \varphi}. \qquad (3.2.24)$$

Laplace's equation for the harmonic potential takes the form

$$\nabla^2 \phi \equiv \frac{\partial^2 \phi}{\partial x^2} + \frac{1}{\sigma} \frac{\partial}{\partial \sigma} \left(\sigma \frac{\partial \phi}{\partial \sigma} \right) + \frac{1}{\sigma^2} \frac{\partial^2 \phi}{\partial \varphi^2} = 0. \qquad (3.2.25)$$

If a flow is axisymmetric, the velocity potential is a function of x and σ but not φ, as required for u_φ to vanish.

3.2.6   Spherical polar coordinates

Consider a three-dimensional irrotational flow and introduce spherical polar coordinates, (r, θ, φ), as shown in Figure 1.3.3. Using relations (2.1.45), we find that the spherical polar components of the velocity are given by

$$u_r = \frac{\partial \phi}{\partial r}, \qquad u_\theta = \frac{1}{r} \frac{\partial \phi}{\partial \theta}, \qquad u_\varphi = \frac{1}{r \sin \theta} \frac{\partial \phi}{\partial \varphi}. \qquad (3.2.26)$$

Laplace's equation for the harmonic potential takes the form

$$\nabla^2 \phi \equiv \frac{1}{r^2} \frac{\partial}{\partial r} \left(r^2 \frac{\partial \phi}{\partial r} \right) + \frac{1}{r^2 \, \sin \theta} \frac{\partial}{\partial \theta} \left(\sin \theta \frac{\partial \phi}{\partial \theta} \right) + \frac{1}{r^2 \, \sin^2 \theta} \frac{\partial^2 \phi}{\partial \varphi^2} = 0. \qquad (3.2.27)$$

If a flow is axisymmetric, the velocity potential is a function of r and θ but not φ, as required for u_φ to vanish.

3.2.7 *Plane polar coordinates*

Consider a two-dimensional irrotational flow and introduce plane polar coordinates, (r, θ), as shown in Figure 1.3.4. Using relations (2.1.47), we find that the plane polar components of the velocity are

$$u_r = \frac{\partial \phi}{\partial r}, \qquad u_\theta = \frac{1}{r} \frac{\partial \phi}{\partial \theta}. \tag{3.2.28}$$

Laplace's equation for the harmonic potential takes the form

$$\nabla^2 \phi \equiv \frac{1}{r} \frac{\partial}{\partial r} \left(r \frac{\partial \phi}{\partial r} \right) + \frac{1}{r^2} \frac{\partial^2 \phi}{\partial \theta^2} = 0. \tag{3.2.29}$$

Note that this equation derives from (3.2.25) by replacing σ with r and φ with θ, and then discarding the x dependence.

PROBLEMS

3.2.1 *Deriving the velocity potential*

(*a*) Consider a two-dimensional flow with velocity components

$$u_x = U \cos(kx) e^{-ky}, \qquad u_y = -U \sin(kx) e^{-ky}, \tag{3.2.30}$$

where U and k are two constants. Confirm that this flow is irrotational, derive the corresponding velocity potential, investigate whether or not the potential is harmonic, and explain why. Sketch the streamline pattern and discuss the structure of the flow and the physical interpretation of the constant k.

(*b*) Consider a three-dimensional flow with velocity components

$$u_x = U \frac{k_x}{k} \cos(k_x x) \sin(k_y y) e^{-kz}, \qquad u_y = U \frac{k_y}{k} \sin(k_x x) \cos(k_y y) e^{-kz},$$

$$u_z = -U \sin(k_x x) \sin(k_y y) e^{-kz}, \tag{3.2.31}$$

where U, k_x, and k_y, are three constants and $k = (k_x^2 + k_y^2)^{1/2}$. This is the three-dimensional counterpart of the two-dimensional flow discussed in (*a*). Confirm that this flow is irrotational, derive the corresponding velocity potential, investigate whether or not the potential is harmonic, and explain why. Discuss the structure of the flow and the physical interpretation of the constants k_x and k_y.

(*c*) Explain why it is not possible to find a velocity potential for simple shear flow along the x axis varying along the y axis whose velocity components are given by $u_x = \xi y$, $u_y = 0$, and $u_z = 0$, where ξ is a constant with units of inverse time called the shear rate.

3.2.2 *Irrotational flow in cylindrical polar coordinates*

Verify by direct substitution that the potential

$$\phi = Ux \left(1 + \tfrac{1}{2} \frac{a^3}{(x^2 + \sigma^2)^{3/2}} \right) \tag{3.2.32}$$

satisfies Laplace's equation (3.2.25), where U and a are two constants. Discuss the structure of the axisymmetric flow described by this potential.

3.2.3 *Irrotational flow in spherical polar coordinates*

Verify by direct substitution that the potential

$$\phi = Ur\cos\theta\left(1 + \tfrac{1}{2}\,\frac{a^3}{r^3}\right) \tag{3.2.33}$$

satisfies Laplace's equation (3.2.27), where U and a are two constants. Discuss the structure of the axisymmetric flow described by this potential.

3.2.4 *Irrotational flow in plane polar coordinates*

Verify by direct substitution that the potential

$$\phi = Ur\cos\theta\left(1 + \frac{a^2}{r^2}\right) + \frac{\kappa}{2\pi}\theta, \tag{3.2.34}$$

satisfies Laplace's equation (3.2.29), where κ, U, and a are three constants. Discuss the structure of the two-dimensional flow described by this potential.

3.3 Finite-difference methods

In practice, Laplace's equation for a harmonic potential, ϕ, is solved by a variety of numerical methods. To illustrate the implementation of the finite-difference method, we consider a two-dimensional potential flow in the xy plane in a rectangular domain confined between two pairs of parallel straight lines,

$$a_x \leq x \leq b_x, \qquad a_y \leq y \leq b_y, \tag{3.3.1}$$

as illustrated in Figure 3.3.1. The left, bottom, and right walls are impermeable, whereas the top wall is exposed to an external flow.

3.3.1   Boundary conditions

Before attempting to compute the solution, we must specify boundary conditions for the scalar potential, ϕ.

Over the left wall, the unit vector normal to the wall pointing into the fluid is $\mathbf{n} = (1, 0)$. Accordingly, the no-penetration condition (3.2.22) provides us with the Neumann boundary condition

$$\frac{\partial\phi}{\partial x} = 0 \quad \text{at} \quad x = a_x. \tag{3.3.2}$$
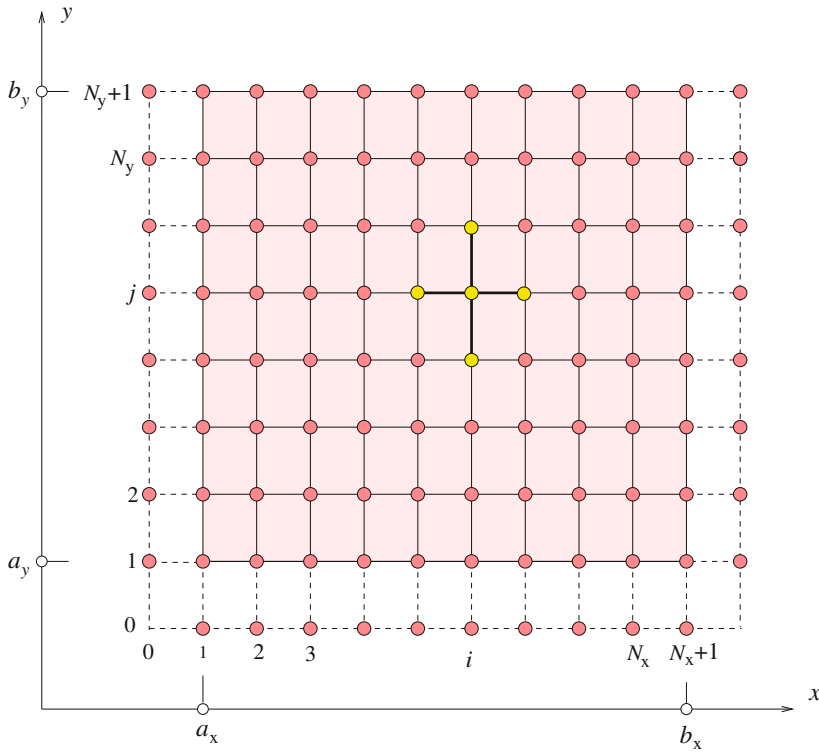
Figure 3.3.1 Illustration of a Cartesian grid used to compute the harmonic potential of a two-dimensional irrotational flow in a rectangular domain. The grid nodes are parametrized by two indices, i and j, where $i = 1, \ldots N_x + 1$ and $j = 1, \ldots N_y + 1$. Phantom grid lines are introduced at $i = 0$, $i = N_x + 2$, and $j = 0$, to implement the Neumann boundary conditions. The solution is found by solving Laplace's equation using a finite-difference method. The five-point stencil indicates the nodal pattern used to approximate the Laplacian at an interior node.

Over the bottom wall, the unit vector normal to the wall pointing into the flow is $\mathbf{n} = (0, 1)$. Accordingly, the no-penetration condition (3.2.22) provides us with the Neumann boundary condition

$$\frac{\partial \phi}{\partial y} = 0 \quad \text{at} \quad y = a_y. \tag{3.3.3}$$

Over the right wall, the unit vector normal to the wall pointing into the flow is $\mathbf{n} = (-1, 0)$. Accordingly, the no-penetration condition (3.2.22) provides us with the Neumann boundary condition

$$\frac{\partial \phi}{\partial x} = 0 \quad \text{at} \quad x = b_x. \tag{3.3.4}$$

Over the top wall, we stipulate for the purpose of illustration that the tangential component of the velocity is constant and equal to V. Other boundary conditions can be imposed to reflect different flow conditions. Since the top wall is parallel to the x axis, the unit tangent vector is $\mathbf{t} = (1, 0)$. Accordingly, expression (3.2.23) provides us with the boundary condition

$$u_t \equiv \mathbf{u} \cdot \mathbf{t} = \frac{\partial \phi}{\partial x} = V \qquad \text{at} \qquad y = b_y. \tag{3.3.5}$$

Straightforward integration of (3.3.5) with respect to x shows that this condition is equivalent to a Dirichlet boundary condition,

$$\phi = Vx + c \qquad \text{at} \qquad y = b_y. \tag{3.3.6}$$

The constant c can be assigned an arbitrary value that is inconsequential to the structure of the flow.

The problem formulation is now complete, and we may proceed to compute the solution. Our task is to solve Laplace's equation

$$\frac{\partial^2 \phi}{\partial x^2} + \frac{\partial^2 \phi}{\partial y^2} = 0, \tag{3.3.7}$$

subject to the four boundary conditions expressed by equations (3.3.2), (3.3.3), (3.3.4), and (3.3.6).

3.3.2   Finite-difference grid

We begin implementing the finite-difference method by dividing the x interval, $[a_x, b_x]$, into N_x evenly spaced sub-intervals separated by the spacing $\Delta x = (b_x - a_x)/N_x$, and draw vertical grid lines at

$$x_i = a_x + (i - 1) \Delta x \tag{3.3.8}$$

for $i = 1, \ldots, N_x + 1$, as shown in Figure 3.3.1.

Similarly, we divide the y interval, $[a_y, b_y]$, into N_y evenly spaced sub-intervals separated by the spacing $\Delta y = (b_y - a_y)/N_y$, and draw horizontal grid lines at

$$y_j = a_y + (j - 1) \Delta y \tag{3.3.9}$$

for $j = 1, \ldots, N_y + 1$, as shown in Figure 3.3.1.

The intersections of vertical and horizontal grid lines define grid points or nodes. For convenience, we denote the value of the harmonic potential ϕ at the (i, j) node as

$$\phi_{i,j} \equiv \phi(x_i, y_j) \tag{3.3.10}$$

for $i = 1, \ldots, N_x + 1$ and $j = 1, \ldots, N_y + 1$.

The Dirichlet boundary condition (3.3.6) provides us with the values

$$\phi_{i,N_y+1} = V x_i. \tag{3.3.11}$$

Without loss of generality, we have made the arbitrary choice $c = 0$. Our objective is to compute the remaining unknown values, $\phi_{i,j}$, at the grid points $i = 1, \ldots, N_x + 1$ and $j = 1, \ldots, N_y$, comprising a set of

$$N_u = (N_x + 1) N_y \tag{3.3.12}$$

unknowns.

3.3.3 Finite-difference discretization

To build a system of equations for the unknown grid values, we require the satisfaction of Laplace's equation (3.2.14) at the (i, j) node, and approximate the second partial derivatives with finite differences. Introducing the approximations implemented in formula (2.5.9), we write

$$\left(\frac{\partial^2 \phi}{\partial x^2}\right)_{i,j} \simeq \frac{\phi_{i-1,j} - 2\phi_{i,j} + \phi_{i+1,j}}{\Delta x^2} \tag{3.3.13}$$

and

$$\left(\frac{\partial^2 \phi}{\partial y^2}\right)_{i,j} \simeq \frac{\phi_{i,j-1} - 2\phi_{i,j} + \phi_{i,j+1}}{\Delta y^2}. \tag{3.3.14}$$

These approximations transform the differential equation (3.3.7) to an algebraic equation,

$$\frac{\phi_{i-1,j} - 2\phi_{i,j} + \phi_{i+1,j}}{\Delta x^2} + \frac{\phi_{i,j-1} - 2\phi_{i,j} + \phi_{i,j+1}}{\Delta y^2} = 0 \tag{3.3.15}$$

at the (i, j) node. Rearranging the left-hand side, we obtain

$$\phi_{i+1,j} - 2(1 + \beta)\phi_{i,j} + \phi_{i-1,j} + \beta\phi_{i,j+1} + \beta\phi_{i,j-1} = 0, \tag{3.3.16}$$

where

$$\beta \equiv (\Delta x/\Delta y)^2 \tag{3.3.17}$$

is the square of the grid spacing ratio. In the case of a square grid, $\beta = 1$.

Equation (3.3.15) and its equivalent equation (3.3.16) can be applied at the interior nodes, $i = 2, \ldots, N_x$ and $j = 2, \ldots N_y$, to obtain a system of

$$N_{\text{fde interior}} = (N_x - 1)(N_y - 1) \tag{3.3.18}$$

difference equations. However, equation (3.3.15) cannot be applied at a boundary node, since one grid point involved in the finite-difference approximation will lie outside the domain of flow. We must somehow generate

$$N_{\text{u}} - N_{\text{fde interior}} = (N_x + 1)N_y - (N_x - 1)(N_y - 1) = N_x + 2N_y - 1 \qquad (3.3.19)$$

additional equations.

Neumann boundary condition

The missing equations originate from the Neumann boundary condition at the left, bottom, and right walls where the no-penetration condition is prescribed. One way of implementing these boundary conditions with an error that is comparable to that of the finite-difference approximations (3.3.13) and (3.3.14), is to extend the domain of solution beyond the physical boundaries of the flow and introduce fictitious or phantom nodes located at

$$x = x_0 = a_x - \Delta x, \qquad y = y_0 = a_y - \Delta y \qquad (3.3.20)$$

at the left and bottom walls, and

$$x = x_{N_x+2} = b_x + \Delta x \qquad (3.3.21)$$

at the right wall. Having introduced these extensions, we apply the second-order finite-difference approximation (2.5.6) to recast the Neumann boundary condition into the discrete form

$$\frac{\phi_{2,j} - \phi_{0,j}}{2\,\Delta x} = 0 \qquad (3.3.22)$$

for $j = 1, \ldots, N_y$, corresponding to the left wall,

$$\frac{\phi_{i,2} - \phi_{i,0}}{2\,\Delta y} = 0 \qquad (3.3.23)$$

for $i = 1, \ldots, N_x + 1$, corresponding to the bottom wall, and

$$\frac{\phi_{N_x+2,j} - \phi_{N_x,j}}{2\,\Delta x} = 0 \qquad (3.3.24)$$

for $j = 1, \ldots, N_y$, corresponding to the right wall.

Algebraic balance

To this end, we pause to confirm that the number of unknowns matches the number of available equations. First, we note that the difference equation (3.3.15) or (3.3.16) may now be applied at the interior and boundary nodes for $i = 1, \ldots, N_x + 1$ and $j = 1, \ldots, N_y$, to yield

$$N_{\text{fde}} = (N_x + 1)\,N_y \qquad (3.3.25)$$

equations. Adding to these equations the

$$N_{\text{bc}} = N_x + 2N_y + 1 \tag{3.3.26}$$

boundary conditions expressed by(3.3.22), (3.3.23), and (3.3.24), we obtain

$$N_{\text{eq}} = (N_x + 1)(N_y + 1) + 2N_y \tag{3.3.27}$$

equations. The total number of equations matches the number of unknowns, including the values of ϕ at the $(N_x + 1)\, N_y$ interior and boundary nodes and the values of ϕ at the $2N_y + N_x + 1$ phantom nodes marked with circular symbols in Figure 3.3.1.

3.3.4   Compilation of a linear system

To formalize the method, we collect the interior and boundary unknowns into a long vector, $\mathbf{w}$, consisting of row-blocks, beginning from the bottom,

$$
\begin{aligned}
\mathbf{w} \quad = \quad \big[\quad & \phi_{1,1}, \phi_{2,1}, \ldots \phi_{N_x+1,1}, \\
& \phi_{1,2}, \phi_{2,2}, \ldots \phi_{N_x+1,2}, \\
& \cdots, \\
& \phi_{1,N_y-1}, \phi_{2,N_y-1}, \ldots \phi_{N_x+1,N_y-1}, \\
& \phi_{1,N_y}, \phi_{2,N_y}, \ldots \phi_{N_x+1,N_y} \quad \big].
\end{aligned}
\tag{3.3.28}
$$

Next, we apply the finite-difference equation (3.3.16) successively at boundary and interior nodes. Without loss of generality, we scan the grid points row-by-row starting from the bottom; a column-by-column compilation would also be acceptable.

Southwestern corner node

For the southwestern corner node $(1, 1)$, we obtain the finite-difference equation

$$\phi_{2,1} - 2\,(1 + \beta)\,\phi_{1,1} + \phi_{0,1} + \beta\,\phi_{1,2} + \beta\,\phi_{1,0} = 0. \tag{3.3.29}$$

Boundary condition (3.3.22) for $j = 1$ requires that $\phi_{2,1} = \phi_{0,1}$, and boundary condition (3.3.21) for $j = 1$ requires that $\phi_{1,2} = \phi_{1,0}$. Using these equations to eliminate $\phi_{0,1}$ and $\phi_{1,0}$ in favor of $\phi_{2,1}$ and $\phi_{1,2}$ on the right-hand side of (3.3.29), we obtain

$$2\,\phi_{2,1} - 2\,(1 + \beta)\,\phi_{1,1} + 2\,\beta\,\phi_{1,2} = 0. \tag{3.3.30}$$

For future reference, we express this equation in the form of the inner product of a vector, $\mathbf{a}^{(1,1)}$, and the vector of unknowns $\mathbf{w}$ defined in (3.3.28), as

$$\mathbf{a}^{(1,1)} \cdot \mathbf{w} = 0, \tag{3.3.31}$$

where

$$\mathbf{a}^{(1,1)} = \big[\, -2(1 + \beta), 2, 0, \ldots, 0 \,\big|\, 2\beta, 0, \ldots, 0 \,\big|\, 0, \ldots, 0 \,\big|\, \ldots \,\big|\, 0, \ldots, 0 \,\big] \tag{3.3.32}$$

is a sparse block vector. Each one of the N_y blocks on the right-hand side of (3.3.32) has $N_x + 1$ entries.

Southwestern bordering node

Next, we consider the boundary node $(2, 1)$ and obtain

$$\phi_{3,1} - 2\,(1+\beta)\,\phi_{2,1} + \phi_{1,1} + \beta\,\phi_{2,2} + \beta\,\phi_{2,0} = 0. \tag{3.3.33}$$

Boundary condition (3.3.23) applied for $i = 2$ requires that $\phi_{2,2} = \phi_{2,0}$. Using this equation to eliminate $\phi_{2,0}$ in favor of $\phi_{2,2}$ on the right-hand side of (3.3.33), we obtain

$$\phi_{3,1} - 2\,(1+\beta)\,\phi_{2,1} + \phi_{1,1} + 2\,\beta\,\phi_{2,2} = 0. \tag{3.3.34}$$

For future reference, we express this equation in the form of an inner vector product,

$$\mathbf{a}^{(2,1)} \cdot \mathbf{w} = 0. \tag{3.3.35}$$

where

$$\mathbf{a}^{(2,1)} = \left[\, 1, -2(1+\beta), 1, 0, \ldots, 0 \,\middle|\, 0, 2\beta, 0, \ldots, 0 \,\middle|\, 0, \ldots, 0 \,\middle|\, \cdots \,\middle|\, 0, \ldots, 0 \,\right] \tag{3.3.36}$$

is a sparse block vector. Each one of the N_y blocks on the right-hand side of (3.3.36) has $N_x + 1$ entries.

Other nodes

Continuing in this fashion, we build the rest of the vectors $\mathbf{a}^{(i,j)}$ for $i = 1, \ldots N_x + 1$ and $j = 1, \ldots N_y - 1$, until we have reached the penultimate row corresponding to $j = N_y$. In simplifying the finite-difference equations for this row, we take into consideration not only the Neumann boundary conditions (3.3.22) and (3.3.24) for the side walls, but also the Dirichlet condition (3.3.11) for the top wall.

For example, considering the northwestern node $(1, N_y)$, we obtain the difference equation

$$-2\,(1+\beta)\,\phi_{1,N_y} + 2\,\phi_{2,N_y} + \beta\,\phi_{1,N_y-1} = -\beta\,V x_1, \tag{3.3.37}$$

which can be expressed in the form of the inner product

$$\mathbf{a}^{(1,N_y)} \cdot \mathbf{w} = -\beta\,V\,x_1, \tag{3.3.38}$$

where

$$\mathbf{a}^{(1,N_y)} = \left[\, 0, \ldots, 0 \,\middle|\, \cdots \,\middle|\, 0, \ldots, 0 \,\middle|\, \beta, 0, \ldots, 0 \,\middle|\, -2(1+\beta), 2, 0, \ldots, 0 \,\right] \tag{3.3.39}$$

is a sparse block vector. Each one of the N_y blocks on the right-hand side of (3.3.39) has $N_x + 1$ entries.

Assembly

Finally, we collect equations (3.3.31), (3.3.35), (3.3.38) and their counterparts for the rest of the interior and boundary nodes into a large system of equations,

$$\mathbf{A} \cdot \mathbf{w} = \mathbf{b}. \tag{3.3.40}$$

The first row of the matrix $\mathbf{A}$ is the vector $\mathbf{a}^{(1,1)}$ defined in (3.3.32); the second row is the vector $\mathbf{a}^{(2,1)}$ defined in (3.3.36); subsequent rows have similar identities. The block vector $\mathbf{b}$ on the right-hand side of (3.3.40) is given by

$$\mathbf{b} = \left[\, 0, \ldots, 0 \,\middle|\, \ldots, \,\middle|\, 0, \ldots, 0 \,\middle|\, -\beta\, V x_1, -\beta\, V x_2, \,\ldots,\, -\beta\, V x_{N_x+1} \,\right]. \tag{3.3.41}$$

The coefficient matrix $\mathbf{A}$ consists of N_y vertical and N_y horizontal partitions in the block tridiagonal form

$$\mathbf{A} = \begin{bmatrix} \mathbf{T} & 2\,\mathbf{D} & \mathbf{0} & \cdots & \mathbf{0} & \mathbf{0} & \mathbf{0} \\ \mathbf{D} & \mathbf{T} & \mathbf{D} & \mathbf{0} & \cdots & \mathbf{0} & \mathbf{0} \\ \mathbf{0} & \mathbf{D} & \mathbf{T} & \mathbf{D} & \mathbf{0} & \cdots & \mathbf{0} \\ \vdots & \vdots & \vdots & \ddots & \vdots & \vdots & \vdots \\ \mathbf{0} & \cdots & \mathbf{0} & \mathbf{D} & \mathbf{T} & \mathbf{D} & \mathbf{0} \\ \mathbf{0} & \mathbf{0} & \cdots & \mathbf{0} & \mathbf{D} & \mathbf{T} & \mathbf{D} \\ \mathbf{0} & \mathbf{0} & \mathbf{0} & \cdots & \mathbf{0} & \mathbf{D} & \mathbf{T} \end{bmatrix}. \tag{3.3.42}$$

The factor *two* in front of the $\mathbf{D}$ block in the first row is due to the Neumann boundary condition. We have introduced the $(N_x + 1) \times (N_x + 1)$ tridiagonal matrix

$$\mathbf{T} = \begin{bmatrix} -2\,(1+\beta) & 2 & 0 & 0 & \cdots & 0 & 0 \\ 1 & -2\,(1+\beta) & 1 & 0 & \cdots & 0 & 0 \\ 0 & 1 & -2\,(1+\beta) & 1 & \cdots & 0 & 0 \\ \vdots & \vdots & \vdots & \ddots & \vdots & \vdots & \vdots \\ \vdots & \vdots & \vdots & \vdots & \ddots & \vdots & \vdots \\ 0 & 0 & \cdots & \cdots & 1 & -2\,(1+\beta) & 1 \\ 0 & 0 & \cdots & \cdots & 0 & 2 & -2\,(1+\beta) \end{bmatrix}, \tag{3.3.43}$$

and the $(N_x + 1) \times (N_x + 1)$ diagonal matrix

$$\mathbf{D} = \begin{bmatrix} \beta & 0 & \cdots & 0 & 0 \\ 0 & \beta & \cdots & 0 & 0 \\ \vdots & \vdots & \ddots & \vdots & \vdots \\ 0 & 0 & \cdots & \beta & 0 \\ 0 & 0 & \cdots & 0 & \beta \end{bmatrix}. \tag{3.3.44}$$

Note that the super- and sub-diagonal elements of $\mathbf{T}$ are equal to unity, except for the elements in the first the last rows that are equal to two. The origin of these irregular elements can be traced back to the Neumann boundary condition. Cursory inspection reveals that all

elements of the matrix **A** are zero, except for the elements along five diagonal lines. Because of the dominant presence of zeros, the matrix **A** is classified as sparse.

The following MATLAB function entitled *cvt_2d_fdm*, located in directory *cvt_2d* inside directory *07_ptf* of FDLIB, generates the coefficient matrix **A** for a specified grid size:

```
function A = cvt_2d_fdm (Nx,Ny,beta)

%-------------------------------
% Generate the coefficient matrix
% of a linear system for the potential
%-------------------------------

N = Ny*(Nx+1);   % matrix size
A = zeros(N,N);
cf = -2.0*(1.0+beta);

%-----------------------
% set the five diagonals
%-----------------------

A(1,1) = cf;   % first row
A(1,2) = 2.0; A(1,Nx+2) = 2.0*beta;

for i=2:Nx+1      % first block
  A(i,i) = cf;
  A(i,i+1) = 1.0;
  A(i,i-1) = 1.0;
  A(i,i+Nx+1) = 2.0*beta;
end

for i=Nx+2:N-Nx-1      % intermediate blocks
  A(i,i) = cf;
  A(i,i+1) = 1.0;
  A(i,i-1) = 1.0;
  A(i,i+Nx+1) = beta;
  A(i,i-Nx-1) = beta;
end

for i=N-Nx:N-1      % last block
  A(i,i) = cf;
  A(i,i+1) = 1.0;
  A(i,i-1) = 1.0;
  A(i,i-Nx-1) = beta;
end

A(N,N) = cf;   % last row
A(N,N-1) = 2.0;
A(N,N-Nx-1) = beta;
```

```
%------------------------------
% reset the ones to twos and
% the faulty betas to zeros
%------------------------------

for i=2:Ny    % run over horizontal partitions
  loc = (i-1)*(Nx+1)+1;
  A(loc,loc-1) = 0.0;
  A(loc,loc+1) = 2.0;
end

for i=1:Ny-1    % run over horizontal partitions
  loc = i*(Nx+1);
  A(loc,loc-1) = 2.0;
  A(loc,loc+1) = 0.0;
end

%-----
% done
%-----

return
```

For $N_x = 2$, $N_y = 3$, and $\beta = 1$, the code generates the matrix:

```
|-4   2   0 |  2   0   0 |  0   0   0 |
| 1  -4   1 |  0   2   0 |  0   0   0 |
| 0   2  -4 |  0   0   2 |  0   0   0 |
| ------------------------------------ |
| 1   0   0 | -4   2   0 |  1   0   0 |
| 0   1   0 |  1  -4   1 |  0   1   0 |
| 0   0   1 |  0   2  -4 |  0   0   1 |
| ------------------------------------ |
| 0   0   0 |  1   0   0 | -4   2   0 |
| 0   0   0 |  0   1   0 |  1  -4   1 |
| 0   0   0 |  0   0   1 |  0   2  -4 |
```

which is consistent with the general form displayed in (3.3.42).

Solving the linear system

We have formulated the problem in terms of the linear system of equations (3.3.40) for the vector **w** defined in (3.3.28). Our next task is to solve this system by numerical methods. Once this has been accomplished, the velocity components at the grid nodes arise as partial derivatives of the potential computed by finite-difference methods.

The following MATLAB code entitled *cvt_2d,* located in directory *07_ptf* of FDLIB, assembles and solves the linear system using a numerical method implemented in an internal MATLAB function invoked by a vector-by-matrix division:

```
ax = 0.0; bx = 1.0;
ay = 0.0; by = 0.4;
veltop = 1.0;
Nx = 16; Ny = 32;

%--------
% prepare
%--------

Dx = (bx-ax)/Nx;    % grid spacing
Dy = (by-ay)/Ny;    % grid spacing
beta = (Dx/Dy)^2;
N = Ny*(Nx+1);    % system size

%------------------
% generate the grid
%------------------

[glx,gly,gx,gy] = grid_2d (ax,bx,ay,by,Nx,Ny);

%-------------------------------------
% specify the potential at the top row
%-------------------------------------

for i=1:Nx+1
  phitop(i) = veltop*glx(i);
end

%-------------------
% coefficient matrix
%-------------------

A = cvt_2d_fdm (Nx,Ny,beta);

%---------------
% right-hand side
%---------------

for i=1:N-Nx-1
  rhs(i) = 0.0;
end

for i=1:Nx+1
  rhs(N-Nx-1+i) = -beta*phitop(i);
end

%-----------------------
% solve the linear system
%-----------------------
```

```
sln = rhs/A';

%-------------------------
% assign solution to nodes
%-------------------------

Ic = 1;    % counter

for j=1:Ny
  for i=1:Nx+1
    ptl(i,j) = sln(Ic);
    Ic = Ic+1;
  end
end

for i=1:Nx+1
  ptl(i,Ny+1) = phitop(i);
end

%-------------
% surface plot
%-------------

surf(glx,gly,ptl')
xlabel('x','fontsize',15)
ylabel('y','fontsize',15)
zlabel('\phi','fontsize',15)

%------------------------------------------
% compute the velocity at the internal nodes
% by numerical differentiation
% using central differences
%------------------------------------------

for i=2:Nx
  for j=2:Ny
    gux(i,j) = (ptl(i+1,j) -ptl(i-1,j)) ...
      /(gx(i+1,j)-gx(i-1,j));
    guy(i,j) = (ptl(i,j+1) -ptl(i,j-1)) ...
      /(gy(i,j+1)-gy(i,j-1));
  end
end

%----------------------------------
% compute the velocity on the walls
% by numerical differentiation
%----------------------------------
```

```
%---
% left wall:  i=1
%---

for j=2:Ny
  gux(1,j) = 0.0;
  guy(1,j) = ( ptl(1,j+1)- ptl(1,j-1)) ...
    /(gy(1,j+1)-gy(1,j-1));
end

%---
% bottom wall:  j=1
%---

for i=2:Nx
  gux(i,1) = ( ptl(i+1,1)- ptl(i-1,1)) ...
    /(gx(i+1,1)-gx(i-1,1));
  guy(i,1) = 0.0;
end

%---
% right wall:  i=Nx+1
%---

for j=2:Ny
  gux(Nx+1,j) = 0.0;
  guy(Nx+1,j) = ( ptl(Nx+1,j+1) -ptl(Nx+1,j-1)) ...
    /(gy(Nx+1,j+1)-gy(Nx+1,j-1));
end

%---
% top wall:  j=Ny+1
%---

for i=2:Nx
  gux(i,Ny+1) = veltop;
  guy(i,Ny+1) = ( ptl(i,Ny+1)- ptl(i,Ny)) ...
    /(gy(i,Ny+1)-gy(i,Ny));
end

%---
% four corners
% velocity is zero or singular;
% set it to zero
%---

gux(1 ,1) = 0.0; gux(Nx+1,1) = 0.0;
gux(1 ,Ny+1) = 0.0; gux(Nx+1,Ny+1) = 0.0;
guy(1 ,1) = 0.0; guy(Nx+1,1) = 0.0;
```
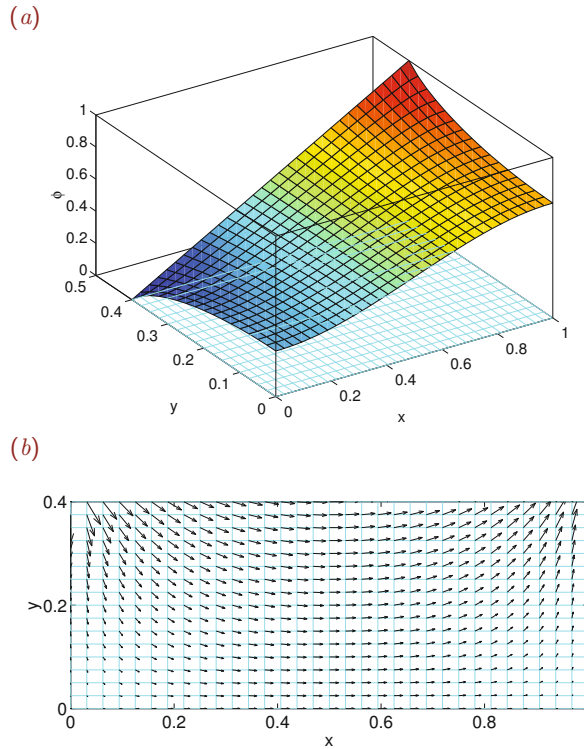
(*a*)

(*b*)

Figure 3.3.2 (*a*) Surface plot of the potential and (*b*) velocity vector field of a two-dimensional potential flow in a rectangular cavity computed by a finite-difference method.

```
guy(1 ,Ny+1) = 0.0; guy(Nx+1,Ny+1) = 0.0;

%---
% graphics
%---

figure
hold on
quiver(gx,gy,gux,guy)
axis equal
xlabel('x','fontsize',15)
ylabel('y','fontsize',15)
box
```

The graphics display generated by the code is shown in Figure 3.3.2. The velocity vector field shown in Figure 3.3.2(*b*) was visualized by the internal MATLAB graphics function *quiver*.

Problems

3.3.1 *Explicit form of a linear system*

Present the explicit form of the linear system (3.3.40) for discretization levels $N_x = 3$ and $N_y = 3$.

3.3.2 *Neumann boundary conditions all around*

Derive the counterpart of the linear system (3.3.40) when the no-penetration boundary condition is applied along all four walls. Specifically, present the components of the unknown vector **w**, constant vector **b**, and coefficient matrix **A**, in a form that is analogous to that displayed in (3.3.42). Then confirm that the sum of the elements in each row of the matrix **A** is zero. Based on this observation, explain why the matrix **A** is singular; that is, its determinant is equal to zero.

3.3.3 ⊠ *Irrotational flow in a cavity*

(*a*) Run the code *cvt_2d* for a cavity with length to depth ratio equal to unity and discretization level as high as you can afford. Plot the velocity vector field and discuss the structure of the flow.

(*b*) Repeat (*a*) for a cavity with length to depth ratio equal to 4.0. Discuss the effect of the cavity aspect ratio on the structure of the flow.

3.4   Linear solvers

In Section 3.3, we reduced the problem of solving Laplace's equation for the harmonic potential in the rectangular domain of a two-dimensional flow to the problem of solving the linear system of equations (3.3.40) for the values of the potential at the nodes of a finite-difference grid deployed over the domain of flow. The reduction was carried out by implementing finite-difference approximations. The solution of the linear system was found using a internal MATLAB function. Since such systems of linear equations arise in broad range of applications within and beyond fluid mechanics, in this section, we review pertinent numerical methods in a generalized framework.

Consider a system of N linear algebraic equations for N unknown scalar variables, $x_1, x_2, \ldots, x_N$,

$$
\begin{aligned}
A_{1,1}\, x_1 + A_{1,2}\, x_2 + \cdots + A_{1,N-1}\, x_{N-1} + A_{1,N}\, x_N &= b_1, \\
A_{2,1}\, x_1 + A_{2,2}\, x_2 + \cdots + A_{2,N-1}\, x_{N-1} + A_{2,N}\, x_N &= b_2, \\
\cdots, \\
A_{N,1}\, x_1 + A_{N,2}\, x_2 + \cdots + A_{N,N-1} x_{N-1} + A_{N,N}\, x_N &= b_N,
\end{aligned}
\tag{3.4.1}
$$

where $A_{i,j}$ for $i, j = 1, \ldots, N$ are given coefficients and b_i are given constants. In matrix notation, the system takes the compact form

$$
\mathbf{A} \cdot \mathbf{x} = \mathbf{b},
\tag{3.4.2}
$$

where $\mathbf{A}$ is an $N \times N$ coefficient matrix,

$$\mathbf{A} = \begin{bmatrix} A_{1,1} & A_{1,2} & \cdots & A_{1,N-1} & A_{1,N} \\ A_{2,1} & A_{2,2} & \cdots & A_{2,N-1} & A_{2,N} \\ \vdots & \vdots & \ddots & \vdots & \vdots \\ A_{N-1,1} & A_{N-1,2} & \cdots & A_{N-1,N-1} & A_{N-1,N} \\ A_{N,1} & A_{N,2} & \cdots & A_{N,N-1} & A_{N,N} \end{bmatrix}, \tag{3.4.3}$$

and $\mathbf{b}$ is an N-dimensional vector,

$$\mathbf{b} = \begin{bmatrix} b_1 \\ b_2 \\ \vdots \\ b_{N-1} \\ b_N \end{bmatrix}. \tag{3.4.4}$$

A variety of direct and iterative solution procedures are available.

3.4.1 Gauss elimination

A general procedure for solving system (3.4.2) employs the method of Gauss elimination. The basic idea is to solve the first equation in (3.4.2) for the first unknown, x_1, and use the expression thus obtained to eliminate x_1 from all subsequent equations. We then retain the first equation as is, and replace all subsequent equations with their descendants that do not contain x_1.

At the second stage, we solve the second equation for the second unknown, x_2, and use the expression thus obtained to eliminate x_2 from all subsequent equations. We then retain the first and second equations, and replace all subsequent equations with their descendants that do not contain x_1 or x_2. Continuing in this fashion, we arrive at the last equation, which contains only the last unknown, x_N.

Having completed the elimination, we compute the unknowns by the method of backward substitution. First, we solve the last equation for x_N, which thus becomes a known. Second, we solve the penultimate equation for x_{N-1}, which also becomes a known. Continuing in the backward direction, we scan the reduced system until we have computed all unknowns.

Pivoting

Immediately before the mth equation has been solved for the mth unknown, where $m = 1, \ldots, N-1$, the linear system takes the form shown in Table 3.4.1, where $A_{i,j}^{(m)}$ are intermediate coefficients and $b_i^{(m)}$ are intermediate right-hand sides.

A difficulty arises when the diagonal element, $A_{m,m}^{(m)}$, is nearly or precisely zero, for then we may no longer solve the mth equation for x_m, as required. However, the failure

$$
\begin{bmatrix}
A_{1,1}^{(m)} & A_{1,2}^{(m)} & \cdots & & \cdots & & \cdots & A_{1,N}^{(m)} \\
0 & A_{2,2}^{(m)} & \cdots & & \cdots & & \cdots & A_{2,N}^{(m)} \\
0 & 0 & \cdots & & \cdots & & \cdots & \cdots \\
0 & 0 & A_{m-1,m-1}^{(m)} & A_{m-1,m}^{(m)} & \cdots & & A_{m-1,N}^{(m)} \\
0 & \cdots & 0 & A_{m,m}^{(m)} & \cdots & & A_{m,N}^{(m)} \\
0 & \cdots & 0 & \cdots & \cdots & & \cdots \\
0 & \cdots & 0 & A_{N,m}^{(m)} & \cdots & & A_{N,N}^{(m)}
\end{bmatrix}
\begin{bmatrix}
x_1 \\ x_2 \\ x_3 \\ \vdots \\ \vdots \\ x_{N-1} \\ x_N
\end{bmatrix}
=
\begin{bmatrix}
b_1^{(m)} \\ b_2^{(m)} \\ b_3^{(m)} \\ \vdots \\ \vdots \\ b_{N-1}^{(m)} \\ b_N^{(m)}
\end{bmatrix},
$$

Table 3.4.1   Transient structure of a linear system of equations at the mth stage of Gauss elimination. The first equation of the transient system is the same as the first equation in the original system (3.4.2) for any m. Subsequent equations are different, except at the first stage corresponding to $m = 1$.

of the method does not imply that the linear system does not have a unique solution. To circumvent this difficulty, we simply rearrange the equations or relabel the unknowns so as to bring the mth unknown to the mth equation using the method of pivoting. If there is no way we can make this happen, the matrix $\mathbf{A}$ is singular and the linear system has either no solution or an infinite number of solutions.

In the method of row pivoting, potential difficulties are bypassed by switching the mth equation of the transient system displayed in Table 3.4.1 with the subsequent kth equation, where $k > m$. The value of k is chosen such that $|A_{k,m}^{(m)}|$ is the maximum value of the elements in the mth column below the diagonal, $A_{i,m}^{(m)}$ for $i \geq m$. If $A_{i,m}^{(m)} = 0$ for all $i \geq m$, the matrix $\mathbf{A}$ is singular and the system under consideration does not have a unique solution.

3.4.2   A menagerie of other methods

In practice, the size of system (3.3.40) can be on the order of $10^4 \times 10^4$ or even higher, corresponding to discretization levels N_x and N_y on the order of 10^2. For such large systems, the method of Gauss elimination requires a prohibitive computational time. The practical need for solving systems of large size has motivated the development of a host of powerful methods for general or specific applications.[1]

Iterative methods

Iterative methods are appropriate for sparse systems with large dimensions. The main idea is to split the coefficient matrix, $\mathbf{A}$, into two matrices, $\mathbf{A}'$ and $\mathbf{A}''$, writing

$$\mathbf{A} = \mathbf{A}' - \mathbf{A}'', \tag{3.4.5}$$

and then recast the system (3.4.2) into the form

$$\mathbf{A}' \cdot \mathbf{x} = \mathbf{A}'' \cdot \mathbf{x} + \mathbf{b}. \tag{3.4.6}$$

---

[1]Pozrikidis, C. (2008) *Numerical Computation in Science and Engineering*, Second Edition, Oxford University Press.

The procedure involves guessing the solution, $\mathbf{x}$, computing the right-hand side of (3.4.6), and solving for $\mathbf{x}$ on the left-hand side. The advantage of this approach is that, if the splitting (3.4.5) is done craftily, it much easier to solve (3.4.6) than (3.4.2) for $\mathbf{x}$ on the left-hand side. The computation is repeated until the value of $\mathbf{x}$ used to compute the right-hand side of (3.4.6) is virtually identical to that arising by solving the linear system (3.4.6). Examples of iterative methods are the Jacobi, the Gauss–Seidel, and the successive over-relaxation (SOR) method.

A different class of iterative methods search for the solution vector, $\mathbf{x}$, by making steps in the N-dimensional space toward craftily designed or optimal directions. The multi-grid method is another powerful technique for solving systems of linear equations arising from finite-difference and related discretization.

Directory *03_lin_eq* inside directory *01_num_meth* of FDLIB contains programs that implement the conjugate and biconjugate gradients methods.

PROBLEM

3.4.1 ▣ *Gauss elimination*

Program *gel*, located in directory *03_lin_eq* inside directory *01_num_meth* of FDLIB, solves a system of linear equations using the method of Gauss elimination with row pivoting. Use the program to solve a system of your choice and verify the accuracy of the solution.

3.5 Two-dimensional point sources and point-source dipoles

Laplace's equation for the harmonic velocity potential–equation (3.2.16) for two-dimensional flow or equation (3.2.20) for three-dimensional flow–is linear. This means that if ϕ_1 and ϕ_2 are two harmonic potentials representing two elementary flows, any linear combination of these potentials,

$$\phi = c_1\,\phi_1 + c_2\,\phi_2, \tag{3.5.1}$$

will also be a harmonic potential representing a hybrid flow, where c_1 and c_2 are two arbitrary coefficients.

3.5.1 Function superposition and fundamental solutions

The linearity of Laplace's equation allows us to generate exact and approximate solutions by the method of superposition. The key idea is to introduce a family of harmonic potentials playing the role of basis functions, also called fundamental solutions, and then use them as building blocks to generate further solutions.

For example, if ϕ_1 and ϕ_2 are two such fundamental solutions, a desired solution can be expressed by the right-hand side of (3.5.1), and the two coefficients c_1 and c_2 can be adjusted to satisfy the boundary conditions.

Various families of fundamental solutions are available for flows in infinite or semi-infinite domains, and for singly, doubly, or triply periodic flows. The most general class of fundamental solutions consists of the fundamental singularities of potential flow.

3.5.2   Two-dimensional point source

Imagine that an incompressible fluid is discharged into an infinite pool through the walls of an infinite perforated cylinder, thereby generating a radial flow in the xy plane outward from the inlet point. In plane polar coordinates centered at the point of discharge, $\mathbf{x}_0 = (x_0, y_0)$, the radial and polar components of the velocity at an arbitrary field point, $\mathbf{x} = (x, y)$, are given by

$$u_r(r) = \frac{m}{2\pi} \frac{1}{r}, \qquad u_\theta = 0, \tag{3.5.2}$$

where

$$r = \sqrt{(x - x_0)^2 + (y - y_0)^2} \tag{3.5.3}$$

is the distance of the field point, $\mathbf{x}$, from the discharge point, $\mathbf{x}_0$, and m is a constant expressing the rate of areal discharge. The units of m are velocity multiplied by length.

The flow described by equations (3.5.2) is attributed to a two-dimensional point source, and the rate of areal discharge m is the strength of the point source. If m is negative, we obtain a point source with negative strength described as a point sink.

The radial velocity of the flow due to a point source decays as the inverse of the distance from the point of discharge, r, for the following physical reason. Since the fluid is incompressible, the flow rate Q across any circular loop of arbitrary radius a centered at the point of discharge must be independent of the loop radius. To verify that the velocity field (3.5.2) satisfies this constraint, we use expression (2.6.21) and find that

$$Q = a \int_0^{2\pi} u_r \, d\theta = \frac{m}{2\pi} a \int_0^{2\pi} \frac{1}{r} \, d\theta = \frac{m}{2\pi} a \frac{1}{a} \int_0^{2\pi} d\theta = m, \tag{3.5.4}$$

as required. If we had set, for example, $u_r = m/(2\pi r^k)$, where the exponent k is not equal to unity, the restriction of constant areal flow rate associated with an incompressible fluid would not be satisfied.

Singular behavior of the point source

As the distance from the point source r tends to zero, the right-hand side of the radial velocity in (3.5.2) tends to infinity. This singular behavior is a manifestation of the idealized nature of the flow due to a point source, and explains why the point source is classified as a singularity.

In practice, the flow expressed by (3.5.2) is valid only for $r > b$, where b is the radius of the perforated cylinder discharging the fluid. Extending the domain of flow inward all the way up to the center of the cylinder, located at $\mathbf{x}_0$, we allow for a mathematical singularity.

Velocity potential

The velocity potential of a two-dimensional point source, denoted by $\phi^{2\text{DPS}}$, is related to the velocity components according to equations (3.2.28),

$$u_r = \frac{\partial \phi^{2\text{DPS}}}{\partial r} = \frac{m}{2\pi} \frac{1}{r}, \qquad u_\theta = \frac{\partial \phi^{2\text{DPS}}}{\partial \theta} = 0. \tag{3.5.5}$$

Integrating the first equation and using the second equation to evaluate the integration constant, we find that

$$\phi^{2\text{DPS}} = \frac{m}{2\pi} \ln \frac{r}{\mathcal{L}} = \frac{m}{4\pi} \ln \frac{(x - x_0)^2 + (y - y_0)^2}{\mathcal{L}^2}, \tag{3.5.6}$$

where $\mathcal{L}$ is a specified length introduced to ensure that the argument of the logarithm is dimensionless, as required. Straightforward differentiation confirms that $\phi^{2\text{DPS}}$ satisfies Laplace's equation in two dimensions at every point,

$$\nabla^2 \phi^{2\text{DPS}} = 0, \tag{3.5.7}$$

except at the singular point, $\mathbf{x}_0$, where the potential and its derivatives are not defined.

Cartesian velocity components and stream function

To derive the Cartesian components of the velocity due to a point source, we take the partial derivatives of $\phi^{2\text{DPS}}$ with respect to x or y, and obtain

$$u_x^{2\text{DPS}} = \frac{\partial \phi^{2\text{DPS}}}{\partial x} = \frac{m}{2\pi} \frac{x - x_0}{(x - x_0)^2 + (y - y_0)^2} \tag{3.5.8}$$

and

$$u_y^{2\text{DPS}} = \frac{\partial \phi^{2\text{DPS}}}{\partial y} = \frac{m}{2\pi} \frac{y - y_0}{(x - x_0)^2 + (y - y_0)^2}. \tag{3.5.9}$$

The streamlines of the flow due to a point source are radial straight lines emanating from the singular point, $\mathbf{x}_0$. The associated stream function is

$$\psi^{2\text{DPS}} = \frac{m}{2\pi} \arctan \frac{y - y_0}{x - x_0} + \psi_0, \tag{3.5.10}$$

where ψ_0 is an inconsequential constant. Note that the stream function is a multi-valued function of position.

A point source embedded in uniform flow

As an application, consider the superposition of uniform (streaming) flow along the x axis with velocity U_x, and the flow due to a point source with strength m situated at the origin, $x_0 = 0$ and $y_0 = 0$. Using the potential $\phi = U_x x$ for the streaming flow and the potential

given in (3.5.6) for the point source, we find that the potential of the composite irrotational flow is

$$\phi(\mathbf{x}) = U_x\, x + \frac{m}{4\pi}\, \ln \frac{x^2 + y^2}{\mathcal{L}^2}, \tag{3.5.11}$$

where $\mathcal{L}$ is an arbitrary length. The associated Cartesian components of the velocity are given by

$$u_x = U_x + \frac{m}{2\pi}\, \frac{x}{x^2 + y^2}, \qquad u_y = \frac{m}{2\pi}\, \frac{y}{x^2 + y^2}. \tag{3.5.12}$$

Note the absence of the inconsequential reference length, $\mathcal{L}$.

To study the structure of the flow, we introduce dimensionless variables denoted by a caret (hat),

$$\widehat{x} = \frac{x}{\mathcal{L}}, \qquad \widehat{y} = \frac{y}{\mathcal{L}}, \qquad \widehat{u}_x = \frac{u_x}{U_x}, \qquad \widehat{u}_y = \frac{u_y}{U_x}, \tag{3.5.13}$$

and recast equations (3.5.12) into the dimensionless form

$$\widehat{u}_x = 1 + \beta\, \frac{\widehat{x}}{\widehat{x}^2 + \widehat{y}^2}, \qquad \widehat{u}_y = \beta\, \frac{\widehat{y}}{\widehat{x}^2 + \widehat{y}^2}, \tag{3.5.14}$$

where

$$\beta = \frac{1}{2\pi}\, \frac{m}{\mathcal{L} U_x} \tag{3.5.15}$$

is a dimensionless parameter expressing the strength of the point source relative to the magnitude of the incident flow. Equations (3.5.14) demonstrate that the structure of the flow is determined by the value of the parameter β.

The streamline pattern shown in Figure 3.5.1 for $\beta = 0.25$ reveals that the velocity potential (3.5.11) describes uniform flow along the x axis past a semi-infinite two-dimensional body whose surface can be identified with two streamlines emanating from a stagnation point lying on the negative part of the x axis. Using the first equation in (3.5.14), we find that the x component of the velocity at the x axis is zero when $\widehat{x} = -\beta$. Thus, the larger the value of β, expressing the relative strength of the point source, the farther the stagnation point is located from the origin.

3.5.3   *Two-dimensional point-source dipole*

Next, we consider the flow due to the superposition of a point source with strength m located at a point, $(x_0 + b, y_0)$, and a point sink with strength $-m$ located at the nearby point $(x_0 - b, y_0)$, where b is a specified half distance, as shown in Figure 3.5.2(a).

Using expression (3.5.6), we find that the combined harmonic potential induced by these singularities is given by

$$\phi(\mathbf{x}) = \frac{m}{4\pi}\, \ln \frac{\big(x - (x_0 + b)\big)^2 + (y - y_0)^2}{b^2} - \frac{m}{4\pi} \ln \frac{\big(x - (x_0 - b)\big)^2 + (y - y_0)^2}{b^2}. \tag{3.5.16}$$
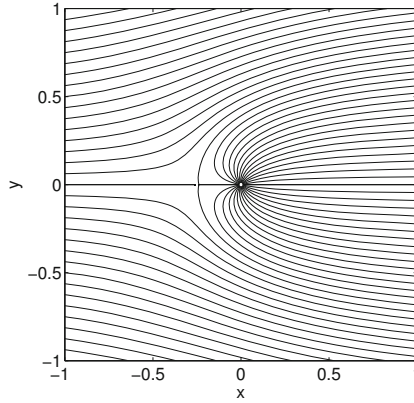
Figure 3.5.1   Streamline pattern of the flow due to the superposition of streaming (uniform) flow along the x axis and the flow due to a two-dimensional point source located at the origin.

Consolidating the logarithms, we obtain

$$\phi(\mathbf{x}) = \frac{m}{4\pi} \, \ln \frac{\left(x - (x_0 + b)\right)^2 + (y - y_0)^2}{\left(x - (x_0 - b)\right)^2 + (y - y_0)^2}. \tag{3.5.17}$$

The Cartesian components of the fluid velocity are found by differentiation,

$$u_x = \frac{\partial \phi}{\partial x} = \frac{m}{2\pi} \left(\frac{x - (x_0 + b)}{\left(x - (x_0 + b)\right)^2 + (y - y_0)^2} - \frac{x - (x_0 - b)}{\left(x - (x_0 - b)\right)^2 + (y - y_0)^2} \right) \tag{3.5.18}$$

and

$$u_y = \frac{\partial \phi}{\partial y} = \frac{m}{2\pi} \left(\frac{y - y_0}{\left(x - (x_0 + b)\right)^2 + (y - y_0)^2} - \frac{y - y_0}{\left(x - (x_0 - b)\right)^2 + (y - y_0)^2} \right). \tag{3.5.19}$$

Now we hold the position of the field point (x, y) fixed and decrease the distance between the two singularities, that is, we let b tend to zero. In this limit, the flow due to the point sink tends to cancel the flow due to the point source. However, if the strengths of the point source and the point sink, $\pm m$, also increase in inverse proportion with the distance between the two singularities, $2b$, then a nontrivial flow due to a point source dipole arises in the limit.

To derive the flow due to a point-source dipole, we recast the expression for the potential on the right-hand side of (3.5.17) into the form

$$\phi(\mathbf{x}) = \frac{m}{4\pi} \left(\ln \left(1 - b \, \frac{2\,(x - x_0) - b}{(x - x_0)^2 + (y - y_0)^2} \right) - \ln \left(1 + b \, \frac{2\,(x - x_0) + b}{(x - x_0)^2 + (y - y_0)^2} \right) \right), \tag{3.5.20}$$

(a)

(b)
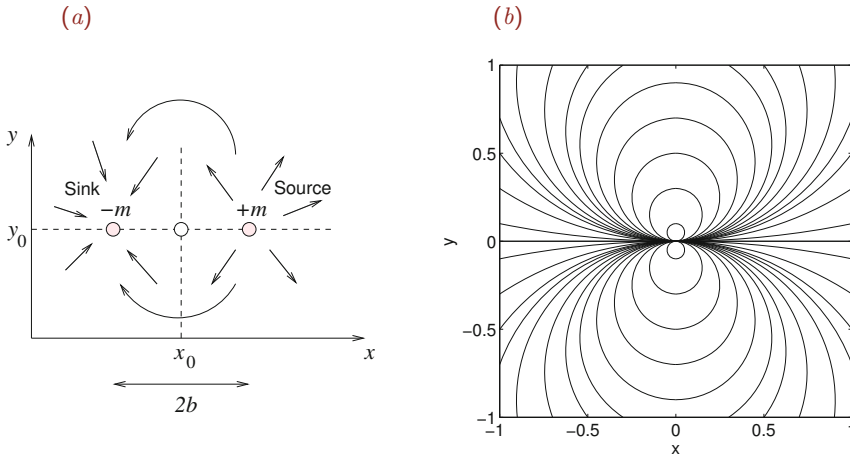
Figure 3.5.2 (a) A point source and a point sink merge to yield a point-source dipole. The depicted dipole is oriented along the x axis. (b) Streamline pattern due to a two-dimensional dipole pointing along the x axis.

and then

$$\phi = \frac{m}{4\pi} \left(\ln(1 - \epsilon_1) - \ln(1 + \epsilon_2) \right), \tag{3.5.21}$$

where

$$\epsilon_1 \equiv b \, \frac{2\,(x - x_0) - b}{(x - x_0)^2 + (y - y_0)^2}, \qquad \epsilon_2 \equiv b \, \frac{2\,(x - x_0) + b}{(x - x_0)^2 + (y - y_0)^2} \tag{3.5.22}$$

are dimensionless variables. As the distance, b, becomes decreasingly smaller than the distance between the field point, $\mathbf{x}$, and the point $\mathbf{x}_0$, both ϵ_1 and ϵ_2 tend to zero.

The Taylor series expansion of the logarithmic function $\ln w$ about the point $w = 1$ provides us with the approximations

$$\ln(1 - \epsilon_1) = -\epsilon_1 + \cdots, \qquad \ln(1 + \epsilon_2) = \epsilon_2 + \cdots. \tag{3.5.23}$$

Substituting these expressions into the right-hand side of (3.5.21) and neglecting quadratic and higher-order terms represented by the dots, we obtain the velocity potential due to a point-source dipole located at the point (x_0, y_0) and oriented along the x axis,

$$\phi^{\text{2DPSDx}} = -\frac{m}{4\pi}(\epsilon_1 + \epsilon_2) \tag{3.5.24}$$

or

$$\phi^{\text{2DPSDx}} = -\frac{d_x}{2\pi} \, \frac{x - x_0}{(x - x_0)^2 + (y - y_0)^2}, \tag{3.5.25}$$

where

$$d_x \equiv 2mb \tag{3.5.26}$$

is the strength of the dipole.

Now comparing (3.5.6), (3.5.25), and (3.5.26), we obtain

$$\phi^{\text{2DPSDx}} = 2b \, \frac{\partial \phi^{\text{2DPS}}}{\partial x_0}, \tag{3.5.27}$$

which shows that the potential due to a point-source dipole oriented along the x axis arises by differentiating the potential due to a point source with respect to the x coordinate of the singular point, x_0. This property classifies the dipole as a derivative singularity descending from the point source.

Velocity components and stream function

The velocity components associated with a two-dimensional (2D) point-source dipole (PSD) oriented along the x axis are given by

$$u_x^{\text{2DPSDx}} = \frac{\partial \phi^{\text{2DPSDx}}}{\partial x} = 2b \, \frac{\partial^2 \phi^{\text{2DPS}}}{\partial x \, \partial x_0} = -2b \, \frac{\partial^2 \phi^{\text{2DPS}}}{\partial x^2} \tag{3.5.28}$$

and

$$u_y^{\text{2DPSDx}} = \frac{\partial \phi^{\text{2DPSDx}}}{\partial y} = 2b \, \frac{\partial^2 \phi^{\text{2DPS}}}{\partial y \, \partial x_0} = -2b \, \frac{\partial^2 \phi^{\text{2DPS}}}{\partial x \, \partial y}. \tag{3.5.29}$$

Carrying out the differentiations, we obtain

$$u_x^{\text{2DPSDx}} = \frac{d_x}{2\pi} \left(-\frac{1}{(x-x_0)^2 + (y-y_0)^2} + 2 \, \frac{(x-x_0)^2}{\left((x-x_0)^2 + (y-y_0)^2 \right)^2} \right) \tag{3.5.30}$$

and

$$u_y^{\text{2DPSDx}} = \frac{d_x}{2\pi} \, 2 \, \frac{(x-x_0)(y-y_0)}{\left((x-x_0)^2 + (y-y_0)^2 \right)^2}. \tag{3.5.31}$$

The associated streamline pattern is shown in Figure 3.5.2(b). The stream function is given by

$$\psi^{\text{2DPSDx}} = \frac{d_x}{2\pi} \, \frac{y-y_0}{(x-x_0)^2 + (y-y_0)^2} + \psi_0, \tag{3.5.32}$$

where ψ_0 is an inconsequential constant.

Dipole along the y axis

Working in a similar fashion, we derive the flow due to a point-source dipole with strength d_y oriented along the y axis. The associated harmonic potential is

$$\phi^{2\text{DPSDy}} = 2b\, \frac{\partial \phi^{2\text{DPS}}}{\partial y_0} = -\frac{d_y}{2\pi}\, \frac{y - y_0}{(x - x_0)^2 + (y - y_0)^2}, \tag{3.5.33}$$

where $d_y = 2mb$ is the strength of the dipole. The corresponding Cartesian components of the velocity are given by

$$u_x^{2\text{DPSDy}} = \frac{\partial \phi^{2\text{DPSDy}}}{\partial x} = 2b\, \frac{\partial^2 \phi^{2\text{DPS}}}{\partial x\, \partial y_0} = -2b\, \frac{\partial^2 \phi^{2\text{DPS}}}{\partial x\, \partial y} \tag{3.5.34}$$

and

$$u_y^{2\text{DPSDy}} = \frac{\partial \phi^{2\text{DPSDy}}}{\partial y} = 2b\, \frac{\partial^2 \phi^{2\text{DPS}}}{\partial y\, \partial y_0} = -2b\, \frac{\partial^2 \phi^{2\text{DPS}}}{\partial y^2}. \tag{3.5.35}$$

Carrying out the differentiations, we obtain the explicit expressions

$$u_x^{2\text{DPSDy}} = \frac{d_y}{2\pi}\, 2\, \frac{(x - x_0)(y - y_0)}{\big((x - x_0)^2 + (y - y_0)^2\big)^2} \tag{3.5.36}$$

and

$$u_x^{2\text{DPSDy}} = \frac{d_y}{2\pi}\left(-\frac{1}{(x - x_0)^2 + (y - y_0)^2} + 2\, \frac{(y - y_0)^2}{\big((x - x_0)^2 + (y - y_0)^2\big)^2} \right). \tag{3.5.37}$$

The streamline pattern is found by rotating the pattern shown in Figure 3.5.2(b) by 90° around the location of the dipole. The stream function is given by

$$\psi^{2\text{DPSDy}} = -\frac{d_y}{2\pi}\, \frac{x - x_0}{(x - x_0)^2 + (y - y_0)^2} + \psi_0, \tag{3.5.38}$$

where ψ_0 is an inconsequential constant.

General dipole orientation

Combining the expressions given in (3.5.25) and (3.5.33), we find that the harmonic potential due to a potential dipole with vectorial strength $\mathbf{d} \equiv (d_x, d_y)$ located at the point $\mathbf{x}_0$ is given by

$$\phi^{2\text{DPSD}} = \mathbf{d} \cdot \mathbf{\Phi}^{2\text{DPSD}}, \tag{3.5.39}$$

where the vector function $\mathbf{\Phi}^{2\text{DPSD}}$ is defined as

$$\mathbf{\Phi}^{2\text{DPSD}} \equiv -\frac{1}{2\pi}\, \frac{1}{(x - x_0)^2 + (y - y_0)^2} \begin{bmatrix} x - x_0 \\ y - y_0 \end{bmatrix}. \tag{3.5.40}$$

The velocity field can be expressed in the corresponding form

$$\mathbf{u} = -\mathbf{d} \cdot \mathbf{U}^{2\text{DPSD}}, \tag{3.5.41}$$

where $\mathbf{U}^{2\text{DPSD}}$ is a 2×2 matrix function of position (Problem 3.5.2).

3.5.4   *Flow past a circular cylinder*

As an application, we consider the superposition of uniform (streaming) flow along the x axis with velocity U_x, and the flow due to a point-source dipole oriented along the x axis located at the origin. Using the potential $\phi = U_x x$ for the streaming flow and the potential given in (3.5.25) with $x_0 = 0$ and $y_0 = 0$ for the dipole, we derive the potential of the composite flow,

$$\phi(x, y) = U_x\, x - \frac{d_x}{2\pi} \frac{x}{x^2 + y^2} = U_x\, x \left(1 - \frac{1}{2\pi} \frac{d_x}{U_x} \frac{1}{r^2} \right),$$ (3.5.42)

where

$$r = \sqrt{x^2 + y^2}$$ (3.5.43)

is the distance of the field point, $\mathbf{x} = (x, y)$, from the center of the cylinder. In plane polar coordinates, (r, θ),

$$\phi(r, \theta) = U_x \left(r - \frac{1}{2\pi} \frac{d_x}{U_x} \frac{1}{r} \right) \cos\theta,$$ (3.5.44)

where the polar angle θ is measured in the counterclockwise direction around the center of the cylinder, defined such that $x = r \cos\theta$.

Now using the expression for the radial component of the velocity in terms of the potential given in the first of equations (3.2.28), we find that

$$u_r = \frac{\partial \phi}{\partial r} = U_x \left(1 + \frac{1}{2\pi} \frac{d_x}{U_x} \frac{1}{r^2} \right) \cos\theta.$$ (3.5.45)

The expression inside the parentheses on the right-hand side is zero at the radial distance

$$r = \left(-\frac{1}{2\pi} \frac{d_x}{U_x} \right)^{1/2},$$ (3.5.46)

where the quantity under the square root is assumed positive. Conversely, if the strength of the dipole has the value

$$d_x = -2\pi\, U_x\, a^2,$$ (3.5.47)

then the radial velocity will be zero at the radial distance $r = a$. The negative sign underlines that the dipole is oriented against the incident streaming flow.

It is evident that the potential (3.5.44) with d_x evaluated from expression (3.5.47) describes uniform flow with velocity U_x past a circular cylinder of radius a centered at the origin, where the no-penetration condition is satisfied over the surface of the cylinder. Substituting the value for d_x given in (3.5.47) into (3.5.44), we derive the explicit solution

$$\phi = U_x \left(r + \frac{a^2}{r} \right) \cos\theta.$$ (3.5.48)

(a)   (b)
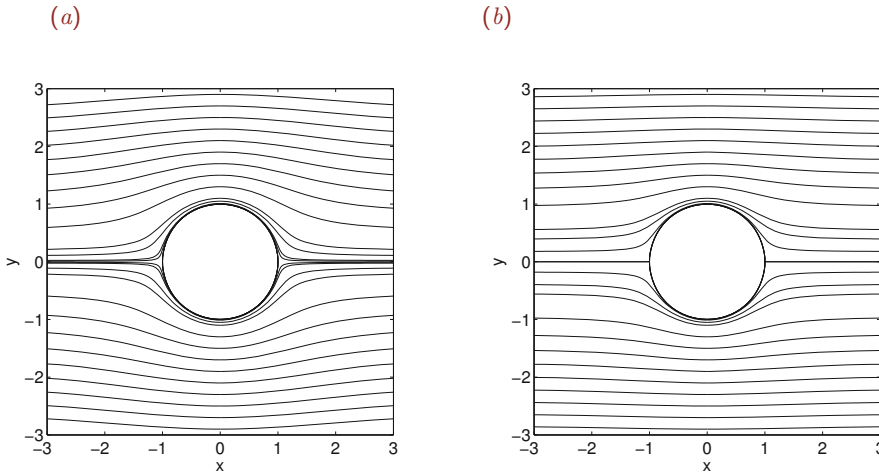
Figure 3.5.3   Streamline pattern of (a) uniform (streaming) flow past a circular cylinder with vanish-
ing circulation around the cylinder, and (b) uniform (streaming) flow past a sphere.

The corresponding Cartesian velocity components are

$$u_x = U_x \left(1 + \frac{a^2}{r^4} - 2\,\frac{a^2}{r^2}\,x^2 \right), \qquad u_y = -2\,U_x\,\frac{a^2}{r^4}\,xy. \tag{3.5.49}$$

The associated streamline pattern is shown in Figure 3.5.3(a). We recall that the origin has
been set at the center of the cylinder and the solution applies in the exterior of the cylinder,
$r \geq a$.

3.5.5   Sources and dipoles in the presence of boundaries

When the domain of flow is bounded by an impermeable surface, the flow due to a point
source or point source dipole must be accompanied with a complementary flow whose pur-
pose is to satisfy the no-penetration boundary condition. For simple boundary geometries,
the complementary flow can be identified with the flow generated by singularities located
at image positions.

Directory *lgf_2d,* located inside directory *07_ptf* of FDLIB, contains a collection of sub-
routines that evaluate the harmonic potential and associated velocity field for several bound-
ary geometries. Two examples are discussed in the remainder of this section.

Point source above a wall

In the case of a point source placed above a plane wall located at $y = y_w$, the complementary
flow is generated by reflecting the point source with respect to the wall. If a primary point
source with strength m is located at a point, (x_0, y_0), then an image point source with equal
strength is located at the point $(x_0, 2y_w - y_0)$. The streamline pattern is shown in Figure
3.5.4(a).

(*a*) (*b*)
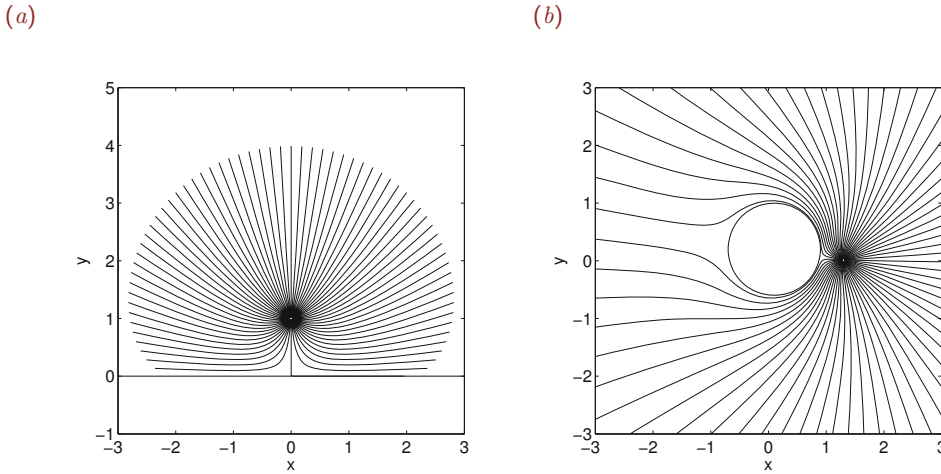
Figure 3.5.4 Streamline pattern of the flow due to a two-dimensional point source (*a*) above a plane wall and (*b*) in front of a circular cylinder.

Point source outside a circular cylinder

In the case of a point source located outside a circular cylinder of radius a centered at a point $\mathbf{x}_c = (x_c, y_c)$, the complementary flow is generated by two image point sources. The first image point source is located at the inverse point of the primary point source with respect to the cylinder. If a primary point source with strength m is located at (x_0, y_0), then an image point source with the same strength is located at the point

$$x_0^{\text{image}} = x_c + (x_0 - x_c)\, \frac{a^2}{|\mathbf{x}_0 - \mathbf{x}_c|^2}, \qquad y_0^{\text{image}} = y_c + (y_0 - y_c)\, \frac{a^2}{|\mathbf{x}_0 - \mathbf{x}_c|^2}, \quad (3.5.50)$$

where

$$|\mathbf{x}_0 - \mathbf{x}_c|^2 = (x_0 - x_c)^2 + (y_0 - y_c)^2 \qquad (3.5.51)$$

is the square of the distance of the primary point source from the center of the cylinder. A second image point source with strength $-m$ is located at the center of the cylinder. Note that the sum of the strengths of the image singularities is zero to ensure that a net flow rate across the surface of the cylinder does not arise. The streamline pattern of the induced flow is shown in Figure 3.5.4(*b*).

PROBLEMS

3.5.1 *Oblique streaming flow past a circular cylinder*

Derive an expression for the harmonic potential and Cartesian components of the velocity of oblique streaming flow with uniform velocity, $u_x = U_x$, $u_y = U_y$, past a circular cylinder of radius a centered at the origin.
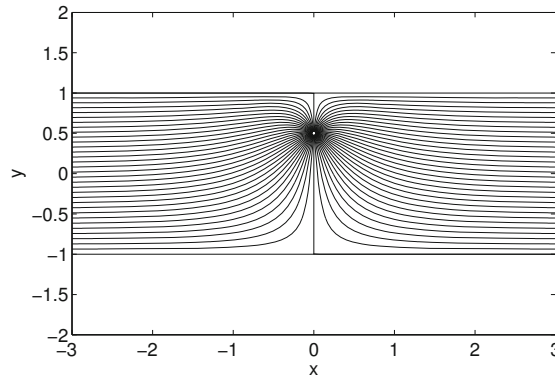
Figure 3.5.5 Streamline pattern of the flow due to a two-dimensional point source between two parallel plates.

3.5.2 *Flow due to a point-source dipole*

Use expressions (3.5.30) and (3.5.36) to derive the explicit form of the matrix $\mathbf{U}^{\text{2DPSD}}$ introduced in (3.5.41).

3.5.3 *Stream functions*

Confirm the stream functions associated with (*a*) a two-dimensional point source given in (3.5.10) and (*b*) a two-dimensional point-source dipole pointing along the x or y axis, given in (3.5.32) and (3.5.38).

3.5.4 🖳 *Point source in a semi-infinite rectangular strip*

Directory *strml,* located inside directory *04_various* of FDLIB, contains a program that generates the streamline pattern of the flow induced by a point source for several boundary geometries. Examples are shown in Figures 3.5.4 and 3.5.5. Run the program to generate the streamline pattern of the flow due to a point source in a semi-infinite rectangular strip and discuss the structure of the flow.

3.6   Three-dimensional point sources and point-source dipoles

The fundamental solutions derived in Section 3.5 for two-dimensional potential flow can be extended in a straightforward fashion to three-dimensional flow.

3.6.1   *Three-dimensional point source*

The harmonic potential due to a three-dimensional point source with strength m located at the point $\mathbf{x}_0 = (x_0, y_0, z_0)$ is

$$\phi^{\text{3DPS}} = -\frac{m}{4\pi} \frac{1}{r}, \tag{3.6.1}$$

where

$$r = \sqrt{(x - x_0)^2 + (y - y_0)^2 + (z - z_0)^2} \qquad (3.6.2)$$

is the distance of the field point, $\mathbf{x}$, from the location of the point source, $\mathbf{x}_0$. The corresponding Cartesian velocity components are

$$u_x^{\text{3DPS}} = \frac{m}{4\pi} \frac{x - x_0}{r^3}, \qquad u_y^{\text{3DPS}} = \frac{m}{4\pi} \frac{y - y_0}{r^3}, \qquad u_z^{\text{3DPS}} = \frac{m}{4\pi} \frac{z - z_0}{r^3}. \qquad (3.6.3)$$

The streamlines are radial straight lines emanating from the singular point, $\mathbf{x}_0$. The fluid moves outward from a point source ($m > 0$) and inward into a point sink ($m < 0$).

3.6.2   Three-dimensional point-source dipole

The harmonic potential due to a three-dimensional point-source dipole oriented along the x, y, or z axis is given, respectively, by

$$\phi^{\text{3DPSDx}} = -\frac{d_x}{4\pi} \frac{x - x_0}{r^3}, \qquad \phi^{\text{3DPSDy}} = -\frac{d_y}{4\pi} \frac{y - y_0}{r^3}, \qquad \phi^{\text{3DPSDz}} = -\frac{d_z}{4\pi} \frac{z - z_0}{r^3}, \qquad (3.6.4)$$

where d_x, d_y, and d_z are the directional strengths of the dipole. The corresponding velocity components are found by straightforward differentiation with respect to x, y, or z.

For a dipole oriented along the x axis, we find that

$$u_x^{\text{3DPSDx}} = \frac{\partial \phi^{\text{3DPSDx}}}{\partial x} = \frac{d_x}{4\pi} \left(-\frac{1}{r^3} + 3 \frac{(x - x_0)^2}{r^5} \right),$$

$$u_y^{\text{3DPSDx}} = \frac{\partial \phi^{\text{3DPSDx}}}{\partial y} = \frac{d_x}{4\pi} 3 \frac{(x - x_0)(y - y_0)}{r^5}, \qquad (3.6.5)$$

$$u_z^{\text{3DPSDx}} = \frac{\partial \phi^{\text{3DPSDx}}}{\partial z} = \frac{d_x}{4\pi} 3 \frac{(x - x_0)(z - z_0)}{r^5}.$$

The streamline pattern in the xy plane is qualitatively similar, but not identical, to that shown in Figure 3.5.2(b) for two-dimensional flow.

For a dipole oriented along the y axis, we find that

$$u_x^{\text{3DPSDy}} = \frac{\partial \phi^{\text{3DPSDy}}}{\partial x} = \frac{d_y}{4\pi} 3 \frac{(y - y_0)(x - x_0)}{r^5},$$

$$u_y^{\text{3DPSDy}} = \frac{\partial \phi^{\text{3DPSDy}}}{\partial y} = \frac{d_y}{4\pi} \left(-\frac{1}{r^3} + 3 \frac{(y - y_0)^2}{r^5} \right), \qquad (3.6.6)$$

$$u_z^{\text{3DPSDy}} = \frac{\partial \phi^{\text{3DPSDy}}}{\partial z} = \frac{d_y}{4\pi} 3 \frac{(y - y_0)(z - z_0)}{r^5}.$$

For a dipole oriented along the z axis, we find that

$$u_x^{3D-PSD-z} = \frac{\partial \phi^{3DPSDz}}{\partial x} = \frac{d_z}{4\pi} \, 3 \, \frac{(z-z_0)(x-x_0)}{r^5},$$

$$u_y^{3D-PSD-z} = \frac{\partial \phi^{3DPSDz}}{\partial y} = \frac{d_z}{4\pi} \, 3 \, \frac{(z-z_0)(y-y_0)}{r^5}, \tag{3.6.7}$$

$$u_z^{3D-PSD-z} = \frac{\partial \phi^{3DPSDz}}{\partial z} = \frac{d_z}{4\pi} \left(-\frac{1}{r^3} + 3 \, \frac{(z-z_0)^2}{r^5} \right).$$

Expressions (3.6.5)–(3.6.7) can be conveniently placed into a compact vector-matrix form, as discussed in Problem 3.6.1.

3.6.3   *Streaming flow past a sphere*

As an application, we consider the superposition of streaming (uniform) flow along the x axis with velocity U_x, and the flow due to a three-dimensional point-source dipole positioned at the origin, $x_0 = 0$, $y_0 = 0$, $z_0 = 0$, and pointing along the x axis.

Using the potential $\phi = U_x x$ for the streaming flow and the first expression in (3.6.4) for the point-source dipole, we find that the potential of the composite axisymmetric flow is given by

$$\phi = U_x \, x - \frac{d_x}{4\pi} \, \frac{x}{r^3} = U_x \, x \left(1 - \frac{d_x}{4\pi U_x} \frac{1}{r^3} \right), \tag{3.6.8}$$

where $r = (x^2 + y^2 + z^2)^{1/2}$ is the distance from the origin. Rearranging, we obtain

$$\phi(r, \theta) = U_x \left(1 - \frac{d_x}{4\pi U_x} \frac{1}{r^3} \right) r \cos \theta, \tag{3.6.9}$$

where θ is the meridional angle defined such that $x = r \cos \theta$.

Using the first expression in (3.2.26), we find that the radial velocity component is given by

$$u_r = \frac{\partial \phi}{\partial r} = U_x \left(1 + \frac{d_x}{2\pi U_x} \frac{1}{r^3} \right) \cos \theta. \tag{3.6.10}$$

The sum inside the parentheses on the right-hand side of (3.6.10) is zero at the radial distance

$$r = \left(-\frac{d_x}{2\pi U_x} \right)^{1/3}. \tag{3.6.11}$$

Conversely, if the strength of the dipole has the value

$$d_x = -2\pi \, U_x \, a^3, \tag{3.6.12}$$

then the radial velocity vanishes at the radial distance $r = a$.

These observations suggest that the potential (3.6.9) with d_x evaluated from expression (3.6.12) describes uniform flow along the x axis with velocity U_x past a stationary sphere of radius a centered at the origin. Substituting (3.6.12) into (3.6.9), we obtain an explicit expression for the potential,

$$\phi = U_x \left(r + \tfrac{1}{2} \frac{a^3}{r^2} \right) \cos\theta. \tag{3.6.13}$$

The corresponding Cartesian velocity components are given by

$$u_x = U_x \left(1 + \tfrac{1}{2} a^3 \left(\frac{1}{r^3} - 3 \frac{x^2}{r^5} \right) \right),$$

$$u_y = -\tfrac{3}{2} U_x a^3 \frac{xy}{r^5}, \qquad u_z = -\tfrac{3}{2} U_x a^3 \frac{xz}{r^5}. \tag{3.6.14}$$

The streamline pattern in an azimuthal plane is shown in Figure 3.5.3(*b*). The structure of the flow is similar to that of flow past a cylinder with zero circulation shown in Figure 3.5.3(*a*).

3.6.4   *Sources and dipoles in the presence of boundaries*

To account for the presence of boundaries, we introduce a complementary flow whose purpose is to ensure the satisfaction of the no-penetration boundary condition, as discussed in Section 3.5.5 for two-dimensional flow. For simple boundary geometries, the complementary flow can be identified with the flow generated by singularities located at image positions outside the domain of flow.

Directory *lgf_3d,* residing inside directory *07_ptf* of FDLIB, contains a collection of sub-routines that evaluate the velocity field for several boundary geometries. The streamline pattern of the flow due to a point source located above a plane wall is shown in Figure 3.6.1(*a*). In this case, the complementary flow is due to a reflected point source. The streamline pattern of the flow due to a point source outside a sphere is shown in Figure 3.6.1(*b*).

PROBLEMS

3.6.1 *Flow due to a three-dimensional point-source dipole*

Express the potential and velocity field of a three-dimensional point source dipole in terms of (*a*) the vectorial strength of the dipole, (*b*) a three-component vector function, $\mathbf{\Phi}^{\mathrm{3DPSD}}$, and (*c*) a 3×3 matrix function, $\mathbf{U}^{\mathrm{3DPSD}}$.

3.6.2 *Stream functions*

Introduce cylindrical polar coordinates with origin at the location of a three-dimensional point source or point-source dipole, and derive expressions for the axisymmetric (Stokes) stream function.

(a)   (b)
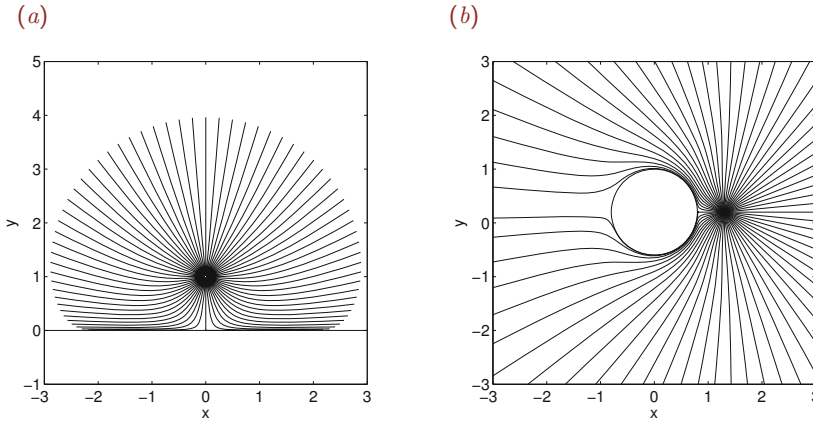
Figure 3.6.1   Streamline pattern in a azimuthal plane of the flow due to a three-dimensional point source (a) above a plane wall or (b) outside a sphere.

3.7   Point vortices and line vortices

Consider a long circular cylinder immersed in an infinite ambient fluid and rotating around its axis with a constant angular velocity, thereby generating a two-dimensional swirling flow in the xy plane.

In plane polar coordinates with origin at the center of the cylinder, $\mathbf{x}_0 = (x_0, y_0)$, the radial and angular velocity components are

$$u_r(\mathbf{x}) = 0, \qquad u_\theta(\mathbf{x}) = \frac{\kappa}{2\pi} \frac{1}{r}, \tag{3.7.1}$$

where

$$r = \sqrt{(x - x_0)^2 + (y - y_0)^2} \tag{3.7.2}$$

is the distance of the point where the velocity is evaluated, $\mathbf{x} = (x, y)$, from the center of the cylinder, and κ is a constant with units of velocity multiplied by length.

The magnitude κ expresses the strength of the flow due to the rotation of the cylinder, and the sign of κ expresses the direction of rotation. If κ is positive, point particles in the flow rotate around the cylinder in the counterclockwise direction. If κ is negative, point particles in the flow rotate around the cylinder in the clockwise direction.

We note that the magnitude of the polar velocity component, u_θ, decays like $1/r$. If the fluid rotated as a rigid body with angular velocity Ω around the point $\mathbf{x}_0$, the polar velocity u_θ would increase linearly with respect to radial distance, as $u_\theta = \Omega r$. It is clear that the velocity field expressed by (3.7.1) represents a flow that is different than rigid-body rotation.
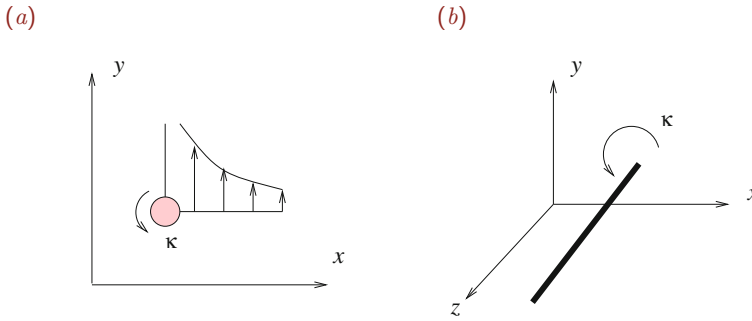
Figure 3.7.1 (a) Two-dimensional and (b) three-dimensional perspectives of a point vortex with positive strength representing a rectilinear line vortex parallel to the z axis.

Point vortex singularity

The flow described by equations (3.7.1) is physically meaningful only in the exterior of the cylinder. Neglecting the surface of the cylinder and extending the domain of flow all the way up to the center of the cylinder, we obtain a singular flow described as the flow due to a point vortex with strength κ, as illustrated in Figure 3.7.1(a). The singularity occurs because, as the distance of an observation point from the point vortex, r, tends to zero, the magnitude of the velocity diverges to infinity.

To confirm that the flow due to a point vortex is irrotational, we substitute expressions (3.7.1) into (2.3.20), and find that the z component of the vorticity vanishes everywhere in the flow, except at the location of the point vortex, $\mathbf{x}_0$, where a singularity appears. These properties classify the point vortex as a singularity of two-dimensional irrotational flow.

A seemingly paradoxical behavior should be noted. Because the flow is irrotational at every point except at the location of the point vortex, small circular fluid parcels not containing the point vortex translate and deform but do not rotate around their center, and yet the fluid exhibits net circulatory motion. The apparent but not essential contradiction serves to underscore that global circulatory motion does not necessarily imply the occurrence of rotational flow.

3.7.1 The potential of irrotational circulatory flow

The presence of circulation has important implications on our ability to describe a flow in terms of a velocity potential. To see this, we use equations (3.2.28) and find that the potential due to a point vortex, denoted by ϕ^{pv}, satisfies the equations

$$\frac{\partial \phi^{\mathrm{pv}}}{\partial r} = 0, \qquad \frac{1}{r}\frac{\partial \phi^{\mathrm{pv}}}{\partial \theta} = \frac{\kappa}{2\pi}\frac{1}{r}. \tag{3.7.3}$$

Integrating these equations, we obtain

$$\phi^{\mathrm{pv}} = \frac{\kappa}{2\pi}\,\theta, \tag{3.7.4}$$

where θ is the polar angle measured around the point vortex in the counterclockwise direction. An arbitrary but irrelevant constant can be added to the right-hand side of (3.7.4). The corresponding stream function is

$$\psi^{\mathrm{pv}} = -\frac{\kappa}{2\pi} \, \ln \frac{r}{\mathcal{L}}, \tag{3.7.5}$$

where $\mathcal{L}$ is a specified length.

According to expression (3.7.4), as we move around the point vortex on a circular path in the counterclockwise direction, the potential increases in proportion to the angle θ. But then, as we return to the point of departure, because θ has increased by 2π, the potential has undergone a jump with respect to the initial value, equal to κ. We can continue traveling around the point vortex for one more turn, only to find that, each time we perform a complete rotation, the potential undergoes a jump equal to κ. This observation illustrates that the potential associated with a point vortex is multi-valued. Moreover, since the point of departure is arbitrary, the potential is multi-valued at every point in the flow.

We have discovered by example that circulatory motion is associated with a multi-valued potential and *vice versa.* In practice, a multi-valued potential is too much to handle by analytical and numerical methods. To circumvent this difficulty, we decompose the potential into an easy multi-valued part and a harder complementary single-valued part; we specify the former, and extract the latter by analytical or numerical methods. The implementation of this method will be discussed in Chapter 12 in the context of aerodynamics.

In an alternative approach, we introduce an artificial boundary residing inside the fluid called a branch cut, and work under the assumption that the potential has two different values on either side of the brunch cut. If the flow does not exhibit net circulatory motion, the two values are identical.

3.7.2   *Flow past a circular cylinder*

To illustrate the usefulness of the point vortex singularity, we consider streaming (uniform) flow past a circular cylinder, as discussed in Section 3.5. Equation (3.5.48) provides us with the single-value harmonic potential in the absence of circulatory motion around the cylinder.

To allow for circulatory motion, we add to the right-hand side of (3.5.48) the potential due to a point vortex situated at the center of cylinder, given in equation (3.7.4), obtaining

$$\phi = U_x \left(r + \frac{a^2}{r} \right) \cos\theta + \frac{\kappa}{2\pi} \, \theta. \tag{3.7.6}$$

The corresponding Cartesian velocity components are

$$u_x = U_x \left(1 + \frac{a^2}{r^2} - 2\frac{x^2}{r^4} a^2 \right) - \frac{\kappa}{2\pi} \frac{y}{r^2}, \qquad u_y = -U_x \, 2\frac{xy}{r^4} a^2 + \frac{\kappa}{2\pi} \frac{x}{r^2}. \tag{3.7.7}$$

Since the radial velocity component, $u_r = \partial\phi/\partial r$, is zero over the surface of the cylinder located at $r = a$, the no-penetration condition is satisfied.

(a)   (b)   (c)
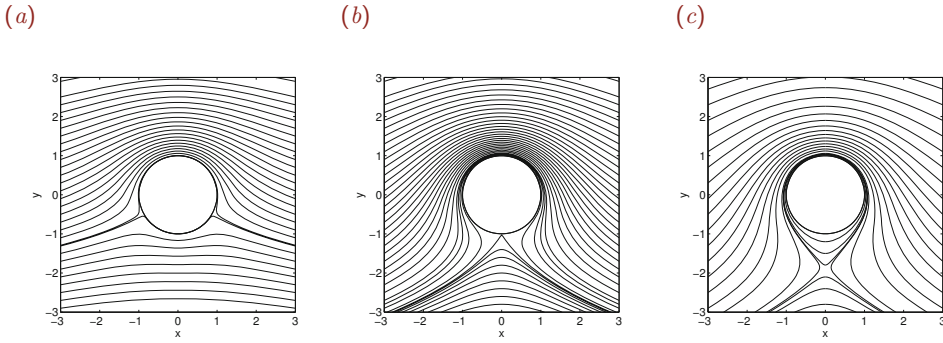
Figure 3.7.2 Streamline pattern of uniform (streaming) flow past a circular cylinder with different degrees of circulation around the cylinder determined by the dimensionless parameter β defined in equation (3.7.9); (a) $\beta = 0.5$, (b) 1.0, and (c) 1.2. The streamline pattern in the absence of circulation, $\beta = 0$, is shown in Figure 3.5.3(a).

Rearranging (3.7.6), we obtain the dimensionless form

$$\phi = U_x a \left(\cos\theta \, (\widehat{r} + \frac{1}{\widehat{r}}) - 2\beta\,\theta \right), \tag{3.7.8}$$

where $\widehat{r} = r/a$ is the scaled radial distance defined such that $\widehat{r} = 1$ corresponds to the cylinder surface, and

$$\beta \equiv -\frac{\kappa}{4\pi V_x a} \tag{3.7.9}$$

is a dimensionless circulation parameter. When $\beta = 0$, the circulation around the cylinder vanishes. Expression (3.7.8) reveals that the structure of the flow is determined by the dimensionless parameter β.

The tangential component of the velocity at the surface of the cylinder is given by

$$u_\theta(r = a) = -2\,V_x\,\sin\theta + \frac{\kappa}{2\pi a} = -2\,V_x\,(\sin\theta + \beta). \tag{3.7.10}$$

We note that the magnitude of the velocity is zero when $\theta = \arcsin(-\beta)$, and conclude that stagnation points develop on the surface on the cylinder when $-1 \leq \beta \leq 1$.

When $\beta = 0$, two stagnation points occur in the horizontal mid-plane of the cylinder located at $\theta = 0$ and π. As β increases from zero to unity, the stagnation points move downward and finally merge at lowest point of the cylinder, $\theta = -\frac{1}{2}\pi$. When β exceeds the value of unity, the merged stagnation points move off the surface of the cylinder into the flow. Streamline patterns for $\beta = 0.5$, 1.0, and 1.2 illustrating this transition are shown in Figure 3.7.2.
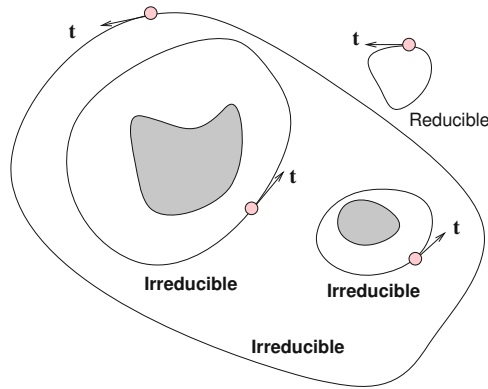
Figure 3.7.3 Illustration of reducible and irreducible loops in a two-dimensional flow. The shaded areas represent flow boundaries.

3.7.3 Circulation

Having discussed the effect of the circulation around a cylinder placed in a uniform flow, we proceed to extend the concept of circulation to a more general framework.

Consider a two-dimensional flow in the xy plane, and draw a simple closed loop inside the flow. If the loop encloses fluid alone and no boundaries, the loop is called reducible. If the loop encloses fluid and one or more boundaries, the loop is called irreducible. The distinguishing feature of a reducible loop is that it can be shrunk to a point without crossing flow boundaries. One reducible and three irreducible loops are depicted in Figure 3.7.3.

Next, we select a point on a reducible or irreducible loop and introduce the unit tangent vector pointing in the counterclockwise direction, $\mathbf{t} = (t_x, t_y)$, as shown in Figure 3.7.3. The inner product of the velocity and the unit tangent vector is given by

$$u_t = \mathbf{u} \cdot \mathbf{t} = u_x\, t_x + u_y\, t_y. \tag{3.7.11}$$

The circulation around the loop is defined as the line integral of the tangential component of the velocity with respect to arc length around the loop, ℓ,

$$C \equiv \oint_{\mathcal{L}} u_t\, \mathrm{d}\ell = \oint_{\mathcal{L}} \mathbf{u} \cdot \mathbf{t}\, \mathrm{d}\ell, \tag{3.7.12}$$

where $\mathcal{L}$ denotes the loop and $\mathrm{d}\ell = \sqrt{\mathrm{d}x^2 + \mathrm{d}y^2}$ is an infinitesimal arc length around the loop.

Reducible loops

Stokes's circulation theorem discussed in Section 11.1 states that, in the absence of point vortices inside the area enclosed by a reducible loop, the circulation around the loop is equal

to the strength of the vorticity integrated over the area of fluid enclosed by the loop, $\mathcal{D}$,

$$C = \iint_{\mathcal{D}} \omega_z \, \mathrm{d}A. \tag{3.7.13}$$

In this case, the right-hand sides of (3.7.12) and (3.7.13) are equal.

An important consequence of Stokes's circulation theorem is that, because the vorticity of an irrotational flow vanishes at every point, the circulation around any reducible loop drawn in an irrotational flow is precisely zero. Important implications of this property will be discussed in Chapter 11 in the context of vortex dynamics.

Reducible loops enclosing point vortices

The circulation around a reducible loop that encloses a collection of N point vortices with strengths $\kappa_1, \kappa_2, \ldots, \kappa_N$ is equal to the sum of the strengths of the point vortices,

$$C = \sum_{i=1}^{N} \kappa_i. \tag{3.7.14}$$

If some point vortices have positive strength and other point vortices have negative strength, so that the sum of the strengths is zero, the circulation around the loop is also zero.

As an example, we consider uniform flow past a circular cylinder described by the potential shown in (3.7.6). To confirm that the circulation around any loop that encloses the cylinder is equal to κ, we compute the circulation around a loop of radius b centered at the cylinder, and find the expected result

$$C \equiv \oint u_t \, \mathrm{d}\ell = \oint u_\theta \, b \, \mathrm{d}\theta = b \oint \frac{1}{r} \frac{\partial \phi}{\partial \theta} \, \mathrm{d}\theta = b \frac{1}{b} \oint \frac{\kappa}{2\pi} \, \mathrm{d}\theta = \kappa, \tag{3.7.15}$$

where $\mathrm{d}\ell = b \, \mathrm{d}\theta$ is the arc length around the loop.

Irreducible loops

The circulation around a loop that encloses one boundary or multiple boundaries in a two-dimensional irrotational flow can be arbitrary. In practice, the amount of circulation is set up internally during a start up period when the flow develops from the state of rest. The circulation established spontaneously around a moving body is of central interest in aerodynamics, as discussed in Chapter 12.

3.7.4   Line vortices in three-dimensional flow

Viewed from a three-dimensional perspective, a point vortex in the xy plane appears like a rectilinear line vortex parallel to the z axis, as shown in Figure 3.7.1(*b*). Deforming this rectilinear line vortex or merging its two ends to form a loop, we obtain a curved three-dimensional line vortex in a three-dimensional flow. One example familiar to cigar smokers is a closed line vortex with a circular or wobbly shape, called a line vortex ring.
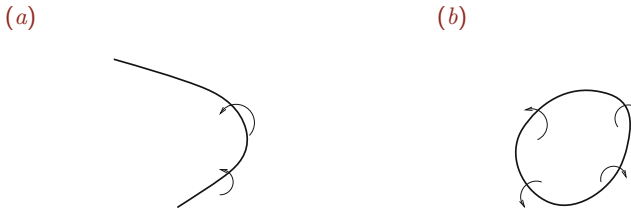
Figure 3.7.4 Illustration of (*a*) an open and (*b*) a closed line vortex in a three-dimensional flow.

A line vortex can be infinite, as illustrated in Figure 3.7.4(*a*), or closed, as illustrated in Figure 3.7.4(*b*). However, a line vortex may not end suddenly in the interior of a fluid. In real life, a fluid is always bounded by a rigid or deformable surface and an otherwise infinite line vortex inevitably ends at the boundaries.

The analysis and computation of the flow associated with, or induced by a three-dimensional line vortex constitutes an important field of fluid mechanics with important applications in turbulent fluid motion and aerodynamics, as discussed in Chapters 11 and 12.

PROBLEMS

3.7.1 *Circulation around a loop in the xy plane*

Consider a closed loop in the xy plane performing m turns around a point vortex with strength κ, where m is an arbitrary integer. Explain why the circulation around this loop is equal to $m\kappa$.

3.7.2 *Point vortex dipole*

Just as the point-source dipole arises from a point source/sink dipole, as discussed in Section 3.5, a point-vortex dipole arises from a point vortex with positive strength and a point vortex with negative strength of equal magnitude, in the limit as the distance between the two point vortices tends to zero while their strength increases by inverse proportion. The harmonic potential associated with a point vortex dipole oriented along the x or y axis is given, respectively, by

$$\phi^{\mathrm{PVDx}}(x,y) = \lambda_x \frac{\partial \phi^{\mathrm{pv}}}{\partial x_0}, \qquad \phi^{\mathrm{PVDy}}(x,y) = \lambda_y \frac{\partial \phi^{\mathrm{pv}}}{\partial y_0}, \qquad (3.7.16)$$

where λ_x and λ_y are the components of the vectorial strength of the point-vortex dipole in the x and y direction.

Carry out the differentiations on the right-hand sides of (3.7.16) and compare the resulting expressions with those shown in equations (3.5.25) and (3.5.33) for the two-dimensional point-source dipole. Based on this comparison, establish a relationship between the flow due to a point-vortex dipole and the flow due to a point-source dipole.

3.7.3 *Irreducible loops in three-dimensional flow*

(*a*) Consider a three-dimensional domain of flow extending to infinity and bounded internally by a toroidal boundary having the shape of a donut. Show that this flow contains irreducible loops that may not be shrunk to a point without crossing flow boundaries.

(*b*) Invent another three-dimensional domain of flow containing irreducible loops.